UPPSALA
UNIVERSITET

Digital Comprehensive Summaries of Uppsala Dissertations from the Faculty of Science and Technology 1551

Wave Loads and Peak Forces on Moored Wave Energy Devices in Tsunamis and Extreme Waves

LINNEA SJÖKVIST

ACTA
UNIVERSITATIS
UPSALIENSIS
UPPSALA
2017

ISSN 1651-6214
ISBN 978-91-513-0054-2
urn:nbn:se:uu:diva-328499

Dissertation presented at Uppsala University to be publicly examined in Polhemsalen, 10134, Ångström, Uppsala, Friday, 20 October 2017 at 09:15 for the degree of Doctor of Philosophy. The examination will be conducted in English. Faculty examiner: Professor Peter Stansby (Manchester University).

Abstract
Sjökvist, L. 2017. Wave Loads and Peak Forces on Moored Wave Energy Devices in Tsunamis and Extreme Waves. *Digital Comprehensive Summaries of Uppsala Dissertations from the Faculty of Science and Technology* 1551. 86 pp. Uppsala: Acta Universitatis Upsaliensis. ISBN 978-91-513-0054-2.

Surface gravity waves carry enormous amounts of energy over our oceans, and if their energy could be harvested to generate electricity, it could make a significant contribution to the worlds power demand. But the survivability of wave energy devices in harsh operating conditions has proven challenging, and for wave energy to be a possibility, peak forces during storms and extreme waves must be studied and the devices behaviour understood. Although the wave power industry has benefited from research and development in traditional offshore industries, there are important differences. Traditional offshore structures are designed to minimize power absorption and to have small motion response, while wave power devices are designed to maximize power absorption and to have a high motion response. This increase the difficulty of the already challenging survivability issue. Further, nonlinear effects such as turbulence and overtopping can not be neglected in harsh operating conditions. In contrast to traditional offshore structures, it is also important to correctly account for the power take off system in a wave energy converter (WEC), as it is strongly coupled to the devices behaviour.

The focus in this thesis is the wave loads and the peak forces that occur when a WEC with a limited stroke length is operated in waves higher than the maximum stroke length. The studied WEC is developed at Uppsala University, Sweden, and consists of a linear generator at the seabed that is directly driven by a surface buoy. A fully nonlinear CFD model is developed in the finite volume software OpenFOAM, and validated with physical wave tank experiments. It is then used to study the motion and the forces on the WEC in extreme waves; high regular waves and during tsunami events, and how the WECs behaviour is influenced by different generator parameters, such as generator damping, friction and the length of the connection line. Further, physical experiments are performed on full scale linear generators, measuring the total speed dependent damping force that can be expected for different loads. The OpenFOAM model is used to study how the measured generator behaviour affects the force in the connection line.

Keywords: OpenFOAM, CFD, Wave power, Tsunami waves, Extreme waves, Offshore

Linnea Sjökvist, Department of Engineering Sciences, Electricity, Box 534, Uppsala University, SE-75121 Uppsala, Sweden.

ISSN 1651-6214
ISBN 978-91-513-0054-2
urn:nbn:se:uu:diva-328499 (http://urn.kb.se/resolve?urn=urn:nbn:se:uu:diva-328499)

- What did the ocean say to the buoy?

...

- Nothing, it just waved.

List of papers

This thesis is based on the following papers, which are referred to in the text by their Roman numerals.

I L. Sjökvist*, J. Wu*, E. Ransley, J. Engström, M. Eriksson and M. Göteman, "Numerical Models for the Motion and Forces of Point-absorbing Wave Energy Converters in Extreme Waves", *Ocean Engineering*, 2017, 145C, pp. 1-14.

II J. Engström*, L. Sjökvist*, M. Göteman, M. Eriksson, M. Hann, E. Ransley, D. Greaves and M. Leijon, "Buoy Geometry and its Influence on Survivability for a Point Absorbing Wave Energy Converter: Scale Experiment and CFD Simulations", *extended abstract presented at the Marine Energy Technical Symposium*, Washington DC, United States of America, May 1-3, 2017.

III L. Sjökvist and M. Göteman, "The Effect of Overtopping Waves on Peak Forces on a Point Absorbing WEC", *Proceedings of the 3rd Asian Wave and Tidal Energy Conference Series*, Singapore, Singapore, October 24-28, 2016.

IV L. Sjökvist, M. Göteman, "Peak Forces on a Point Absorbing Wave Energy Converter Impacted by Tsunami Waves", *under review for Renewable Energy*, 2017.

V L. Sjökvist, M. Göteman and M. Leijon, "Survivability of a Point Absorbing Wave Energy Converter Impacted by Tsunami Waves", *Proceedings of the 12th European Wave and Tidal Energy Conference Series*, Cork, Ireland, August 27-31, 2017.

VI L. Sjökvist and M. Göteman, "Peak Forces on Wave Energy Linear Generators in Tsunami and Extreme waves", *Energies*, 2017, 10(9), 1323.

VII L. Ulvgård*, L. Sjökvist*, M. Göteman and M. Leijon, "Line Force and Damping at Full and Partial Stator Overlap in a Linear Generator for Wave Power", *Journal of Marine Science and Engineering*, 2016, 4(4), 81.

VIII L. Ulvgård, L. Sjökvist and M. Leijon, "Speed Dependent PTO Damping in a Linear Generator for Wave Power - Measured Damping and Simulated WEC Behaviour", *under review for Journal of Marine Science and Engineering*, 2017.

IX A. Frost, L. Ulvgård, L. Sjökvist, S. Eriksson and M. Leijon, "Experimental Study of Generator Damping at Partial Stator Overlap in a Linear Generator for Wave Power", *Proceedings of the 12th European Wave and Tidal Energy Conference Series*, Cork, Ireland, August 27-31, 2017.

X L. Sjökvist, R. Krishna, V. Castellucci, A. Hagnestål, M. Rahm and M. Leijon, "On the Optimization of Point Absorber Buoys", *Journal of Marine Science and Engineering*, 2014, 2(2), pp. 477-492.

XI L. Sjökvist, M. Göteman, M. Rahm, R. Waters, O. Svensson, E. Strömstedt and M. Leijon, "Calculating Buoy Response for a Wave Energy Converter - a Comparsion Between Two Computational Methods and Experimental Results", *Theoretical and Applied Mechanics Letters*, 2017.

Reprints were made with permission from the publishers.

* The first authorship is shared between the first and the second author.

The author has contributed to the following papers which are not included in this thesis.

XII L. Sjökvist, J. Engström, S. Larsson, M. Rahm, J. Isberg and M. Leijon, "Simulation of Hydrodynamical Forces on a Buoy - a Comparsion Between Two Computational Approaches" *Proceedings of the 1st Asian and Tidal Energy Conference Series*, Jeju Island, South Korea, November 27-30, 2012.

XIII Y. Hong, E. Hultman, V. Castellucci, B. Ekergård, L. Sjökvist, D. E. Soman, R. Krishna, K. Haikonen, A. Baudoin, L. Lindblad, E. Lejerskog, D. Käller, M. Rahm, E. Strömstedt, C. Boström, R. Waters and M. Leijon, "Status Update of the Wave Energy Research at Uppsala University" *Proceedings of the 10th European Wave and Tidal Energy Conference Series*, Aalborg, Denmark, September 2-5, 2013.

Contents

Nomenclature

A_{frac}	-	The fraction of the stator overlapped by the translator
F_{line}	[N]	Force in the connection line
F_{PTO}	[N]	Force from the power take off system
$F_{endstop}$	[N]	Force from the endstops
F_{EM}	[N]	Electromagnetic force
F_{fric}	[N]	Frictional force
$\bar{x}_b$	[m]	Position of the buoy
x_t	[m]	Position of the translator
m_b	[kg]	Mass of the buoy
m_t	[kg]	Mass of the translator
S	[m^2]	Wetted surface of the buoy
V	[m^3]	Submerged volume of the buoy
ρ	[kg/m^3]	Density
P	[Pa]	Total pressure
P_{dyn}	[Pa]	Dynamic pressure
P_a	[Pa]	Air pressure at the free surface
γ	[kNs/m]	Generator damping coefficient
f_{el}	[Hz]	Electrical frequency
E_i	[V]	Induced voltage
B	[T]	Magnetic flux density
I	[A]	Current in the stator winding
l	[m]	length of a conductor
U	[V]	Voltage
L_g	[H]	Generator inductance
R_g	[Ω]	Generator resistance
R_l	[Ω]	Resistance in external load
R_{tot}	[Ω]	Total resistance in the circuit
τ	[m]	Pole width
P_{abs}	[W]	Power absorbed from the waves to the buoy
P_{max}	[W]	Maximum power absorbed from the waves to the buoy
P_w	[W]	Power of the incoming waves passing the buoy
P_{mech}	[W]	Mechanical power exerted by the buoy
P_{el}	[W]	Electrical power in the generator
P_{loss}	[W]	Power loss

Continues on next page

$\bar{u}$	[m/s]	Fluid velocity
$\bar{U}$	[m/s]	Mean component of fluid velocity
$\bar{u}'$	[m/s]	Fluctuating component of fluid velocity
ν	[m^2/s]	Fluid viscosity
$\bar{f}$	[N]	External force
Φ		Scalar velocity potential
η	[m]	Surface elevation
k	[m^{-1}]	Wave number
ω	[rad/s]	Wave angular frequency
A	[m]	Wave amplitude
C	[m/s]	Wave phase speed
J	[W/m]	Power transported per meter of a wave front
T_E	[s]	Wave energy period
H_s	[m]	Significant wave height
α	-	Scalar field used to track the free surface
R_r	[Ns/m]	Radiation damping
K	[N/m]	Stiffness of hydrostatic restoring force
F_{ex}	[N]	Excitation force from the waves
$\bar{r}$	[m]	Position vector of the buoy
r	[m]	Distance between the buoy and the anchoring position
$\hat{r}$	-	Unit vector pointing from the buoy position to the anchoring position
l_{free}	[m]	Free stoke length of the translator
l_{total}	[m]	Total stoke length of the translator
δ_{free}	-	Heaviside function used to define the free stroke length
δ_{total}	-	Heaviside function used to define the total stroke length
δ_{down}	-	Heaviside function used to define when the translator stands on the bottom of the translator

Abbreviations

PTO	Power Take-Off
WEC	Wave Energy Converter
RANS	Reynolds-Averaged Navier Stokes
OWC	Oscillating Water Column
Nd-Fe-B	Neodymium-Iron-Boron
FEM	Finite Element Method
FVM	Finite Volume Method
SPH	Smoothed-Particle Hydrodynamics
VOF	Volume Of Fluid Method
CYL	Cylinder buoy
CWM	Cylinder buoy With Moonpool

1. Introduction

Surface gravity waves carry enormous amounts of energy over our oceans, and if the energy could be harvested to generate electricity, it could make a significant contribution to the world's power demand. Wave energy as a resource is renewable, energy dense, and more predictable than for example wind power. However, the power in a storm is several magnitudes higher than during normal operating conditions. For wave energy to be a possibility, peak forces during storms and extreme waves must be studied, and the dynamical behaviour in harsh operating conditions must be understood.

The first wave energy patent was filed already in 1799 by Gerard and Son in France [1]. However, it was not until the oil crisis in the 1970s that funding of research regarding wave power technology started to increase, and thereby the development. Today, a wide range of technologies and concepts are being developed, and a handful of concepts have been tested offshore [2, 3]. Ensuring survivability offshore and still keeping a reasonable manufacturing cost has proven challenging [4, 5], and no device has achieved economic viability yet. Wave power research has initially focused on methods of power extraction and maximizing energy absorption, using potential linear flow theory, and commonly assuming power take-off (PTO) systems to behave as linear springs and damper systems [6]. A very high power extraction has proven possible in theory; for specific operating conditions, even more energy than what is covered by the buoy area is possible to absorbe in resconance [7]. The wave power industry has benefited from research and development in traditional offshore industries, but there are important design differences. Traditional offshore structures are designed to minimize power absorption and to have small motion response, while wave power devices are designed to maximize power absorption and to have a high motion response. This increases the difficulty of the already challenging survivability issue, and the high motion response violates the linear assumption of small motion. Further, nonlinear effects such as turbulence and overtopping can not be neglected. In contrast to traditional offshore structures, it is also important to correctly account for the PTO damping in a wave energy converter (WEC), as it is strongly coupled to the WECs behaviour.

In recent years, several fully nonlinear high-fidelity models have been developed for different wave power devices. However, the dynamics and forces involved are highly dependent on the structure being modelled, and for each unique wave power device a numerical model must be developed and verified.

1.1 Thesis aim

The aim of this thesis is to study the survivability of the wave power concept of Uppsala University, in harsh operating conditions and during tsunami wave events. The WEC utilizes a linear generator on the seabed as PTO, which is directly driven by a point-absorbing buoy at the surface. The linear generator has a limited stroke length, and when it is reached in high waves, a peak force will occur when the translator inside the linear generator hits the upper endstop. The focus of this thesis is to study the force of those endstop hits, and parameters that influence the magnitude of the force. The dynamics of the WEC in harsh operating conditions and during tsunami wave events are also studied.

1.2 Thesis outline

The focus of this doctoral project has been to develop a numerical model in which both the endstop hits and the behaviour of the WEC in harsh operating conditions and in tsunami waves can be studied. A fully nonlinear numerical model has been developed in the open source software OpenFOAM, and validated with physical wave tank experiments. The model has then been used to study the motion and the forces on the WEC in extreme waves; high regular waves and during tsunami events, and how the WEC behaviour is influenced by different generator parameters, such as generator damping, friction and length of the connection line. Since the forces and the motion of the WEC are highly dependent on the generator behaviour, the generator damping of two different full scale linear generators has been studied during onshore experiments. The RANS-VOF model was then used to study the consequences of the discrepancies between the experimentally measured generator behaviour and an assumed linear behaviour. Two papers using linear theory have also been included in this thesis, showing that linear theory is suitable during normal operating conditions, when the endstop is not hit. This thesis is comprised of two parts.

Part I: Background, aims to introduce the research subject and give a theoretical background and a brief literature review. Chapter 2 is an introduction to wave power technology with a focus on the wave power device of Uppsala University. Chapter 3 is a theoretical chapter, which provides the theoretical background of fluid flow and numerical simulations of linear and nonlinear aspects of fluid flows. This is followed by a section that considers the theoretical background of numerical modelling of wave energy converters. Last, a literature study of numerical modelling of tsunami waves is provided.

Part II: Modelling of forces on a point-absorbing wave energy converter is based on the papers included in this thesis. Chapter 4 describes the methods

used in this thesis. Section 4.1 describes the fully nonlinear Reynolds-Average Navier Stokes (RANS) model that has been developed, and in section 4.2, the experiments that were performed on two full scale WEC prototypes are described. Chapter 5 describes and discusses the results of the papers included in this thesis. Section 5.1 compares forces modelled with the RANS model with experimental wave tank data, showing good agreement. In section 5.2, the RANS model is used to study different aspects influencing the peak forces in the connection line during high regular waves, such as buoy geometry, overtopping waves, linear damping and friction. In section 5.3, the WEC survivability in tsunami waves is studied. Section 5.4 considers the nonlinear aspects of the PTO-system, that were experimentally measured for the full scale prototypes. The RANS model is used to study how the discrepancies between the measured PTO behaviour and an assumed linear PTO system influence the peak forces of a WEC. Chapter 6 provides discussion and conclusions. A summary of the papers that this thesis is based on is found in chapter 7.

Part I:
Background

2. Wave power

2.1 Wave power

Wave power technology is not yet a mature industry, and there exist a large number of different concepts. They are commonly divided into groups, in reference [3] Falcao et al. described three groups:

Wave power technologies

I. Oscillating water columns (OWC); where the waves are pressurizing air in a chamber and pressing it through an air turbine that drives a generator. An example of an on-shore OWC is the "Picoplant" [8], while the "Backward Bent Duct Buoy" is a floating OWC [9].
II. Overtopping devices; where the waves are overtopping a reservoir, and the water then flows back to the ocean trough a water turbine. The "Wave Dragon" [10] is a floating overtopping device.
III. Oscillating body systems; where the motion of the waves are used to oscillate rigid bodies. A power take off (PTO) system is needed to transform the motion to power. Hydraulic PTO systems can be used, as well as electrical generators.

The groups are commonly further categorized, for example in bottom mounted or floating structures, semi-submerged or fully submerged structures, onshore, near-shore or offshore structures. Oscillating body systems can be categorized based on the their motion; heaving, pitching, surging, rotating etc. In reference [11], oscillating body systems are categorized as:

Oscillating body systems

I. Attenuators; the device is floating parallel with the wave direction, perpendicular to the wave fronts. Examples are the "Pelamis" [12] and "ANACONDA" [13] concepts.
II. Point-absorbers; where a PTO system is driven by a floating [14] or submerged [15] buoy that is small in comparison to the wave length. As a consequence of their small dimensions they are omnidirectional. They will also have a resonance frequency where they possibly can absorb even more energy than is passing the buoy [16].
III. Terminators; where the structure is aligned parallel to the wave front, and theoretically can absorb all the wave energy and "terminating" the wave. "Salter's Duck" [17] is a famous example of a terminating wave power concept.

This thesis is focused on the point-absorbing wave power concept developed at Uppsala University, Sweden, which will be further described in section 2.2.

2.2 The wave power concept of Uppsala University

At Uppsala University, Sweden, a wave power concept has been developed since 2002 and several patents have been filed. The wave power device consists of a linear generator placed at the seabed, that is directly driven by a semi-submerged point-absorbing buoy at the sea surface connected with a steel line. Inside the generator, a translator with permanent magnets are moving inside a stator winding, generating electricity. The translator rolls on rubber coated wheels to keep it centered. In 2006, the first prototype, referred to as L1, was deployed and operated off-shore at the Lysekil test site at the west coast of Sweden [18, 19, 20, 21]. Since then, several prototypes have been deployed, both at the Lysekil test site and at the Hammarudda test site in the archipelago at the east coast of Sweden.

The prototype L1 was operated both individualy [22, 23, 24, 25] and in a park together with the prototypes L2 and L3 [26]. An underwater substation was developed and used for the park operation [27, 28, 29]. For the L1, L2 and L3 prototypes, retraction springs were used to pull the translator down in the wave trough. For the newer models, gravity is the only retraction force, and the mass of the translator has been increased to increase the retraction force [30]. Other examples of product developement includes the electrical design of the control system [31, 32, 33, 34] and a change of magnetic material of the translator; the magnetic material in prototype L1 to L10 is Neodymium-Iron-Boron (Nd-Fe-B), while ferrite is used for later prototypes [35].

2.2.1 Motion and forces on the WEC

The generator prototype L10 is seen in figure 2.1, together with a schematic figure of how the translator moves inside the generator hull. As a consequence of the linear machine, the translator motion is restrained by an upper and a lower endstop, limiting the stroke length. Endstop springs are used to dampen the motion before the endstop is hit, to decrease the peak force of an endstop hit. If a wave peak is high enough to lift the translator to exceed the free stroke length, as seen in figure 2.1 b), a peak force will occur when the endstop spring is hit. If the wave is high enough for the translator to reach the total stoke length, the endstop spring is fully compressed and a second peak force occurs. The magnitude of the peak forces depend on the motion of the translator as well as the spring constant of the endstop spring and the elasticity of the connection line.

The dynamic behaviour of the WEC when deployed offshore is described by the equations of motion for the buoy and the translator respectively, Eq. (2.1) and Eq. (2.2). The translator and buoy are connected by the line force F_{line}, which drives the motion of the translator. When the connection line

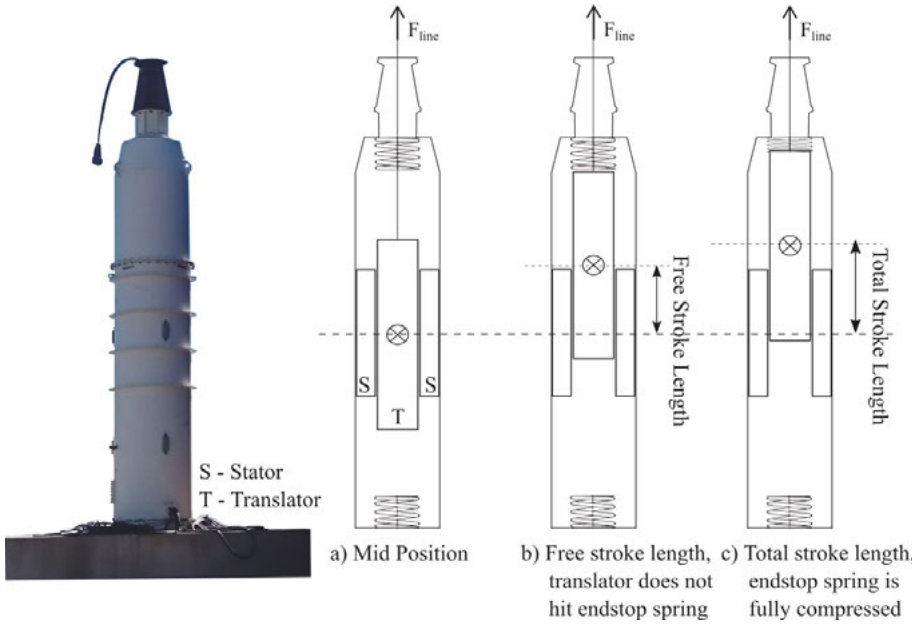

Figure 2.1. The linear generator is placed on the seabed. The translator is moving inside the stator, and electricity is generated in the stator windings. a) The translator in middle position. b) Free stroke length, translator does not compress the endstop spring. c) Total stroke length, the endstop spring is fully compressed.

is stretched, the equations are coupled by F_{line}, and when the line is slack, $F_{line} = 0$. The buoy moves in six degrees of freedom, while the translator is restrained to vertical movement.

$$m_b \ddot{\bar{x}}_b(t) = \int P_{dyn} d\bar{S} - \rho \bar{g} V(\bar{x}_b) + m_b \bar{g} - \bar{F}_{line}, \tag{2.1}$$

$$m_t \ddot{\bar{x}}_t(t) = \bar{F}_{line} - \bar{F}_{PTO} + m_t \bar{g} \pm F_{endstop}, \tag{2.2}$$

where $\bar{x}_b$ and x_t represent the position of the buoy and the translator. The buoy mass and translator mass are described by m_b and m_t. In Eq. (2.1), $\int P_{dyn} d\bar{S}$ and $\rho \bar{g} V(\bar{x})$ represent the hydrodynamic and the hydrostatic force, where $V(\bar{x})$ is the submerged volume, ρ is the water density and P_{dyn} is the dynamical pressure. The PTO force, F_{PTO}, represents the damping of the generator. When the translator hits the upper or lower endstop springs, endstop forces will be added, $F_{endstop}$. A unique property of a linear generator is that the translator-stator overlap can be partial, as can be seen in figure 2.1. In Eq. 2.2, this must be compensated for by multiplying F_{PTO} with a factor A^c_{frac}, where A_{frac} is the fraction of the stator covered by the translator. In figure 2.1 (a), $A_{frac} = 1$, and in figure 2.1 (b) and (c), A_{frac} is less than 1.

A linear model of the force in the connection line was developed by Eriksson et al. [36, 37] which showed good agreement in the frequency domain with an offshore experiment where a buoy was moored with linear springs. Linear models are fast and show good agreement during normal operating conditions, and are suitable for optimization and wave-to-wire modelling [38, 39, 40, 41, 42]. However, nonlinear effects such as overtopping and turbulence must be considered in harsh operation conditions and extreme wave events, such as storm surges and tsunami waves. The line force has been measured offshore in both full scale, during normal operating conditions [19, 43], and in scaled model tests with linear springs instead of a generator in more energetic sea states [44]. The forces in the inner framework of the generator and the lateral forces have been measured offshore by Savin et al. [45, 46, 47], and Gravråkmo compared a cylinder buoy and a torus shaped buoy [48]. However, although offshore experiments are necessary for proving a concept before commercialization, it does not provide the controlled environment needed to make a qualitative analysis of specific parameters. The peak force of endstop hits are studied in a 1:20 scaled physical wave tank experiment by Göteman et al. [49], where the PTO force was approximated as friction damping, and the endstop forces were seen to decrease with increased friction damping.

2.2.2 Generator damping

The PTO system of a WEC is commonly characterized by a constant damping factor γ, so that the PTO force is described as $F_{PTO} = \gamma \dot{x}$, where $\dot{x}$ is the speed of the moving parts of the system. In the Uppsala University WEC, $\dot{x}_t$ is the speed of the translator as it moves inside the stator in the generator. When the connection line is tense, $\dot{x}_t$ equals the speed of the buoy in the direction pointing towards the connection point at the generator. When the translator with permanent magnets moves inside the stator, the stator windings are exposed to a magnetic field $\bar{B}$ and there will be an electromagnetic damping force in the generator. If the conductor has the length l, the Lorentz force is [50]:

$$\bar{F}_{EM} = (\bar{B} \times \bar{I}) l. \tag{2.3}$$

It can be seen that F_{EM}, and consequently also F_{PTO}, depends on generator design parameters and the connected load. The mechanical power, force and damping are directly connected as:

$$\gamma = \frac{F_{PTO}^{mech}}{\dot{x}_b} = \frac{P_{mech}}{{\dot{x}_b}^2}, \tag{2.4}$$

where $\dot{x}_b$ is the speed of the buoy and P_{mech} is the mechanical power exerted by the buoy, $P_{mech} = F_{line} \dot{x}_b$. If assuming an ideal generator without losses and that $\dot{x}_t = \dot{x}_b$, then P_{mech} equals P_{el}, and the ideal damping and PTO force can

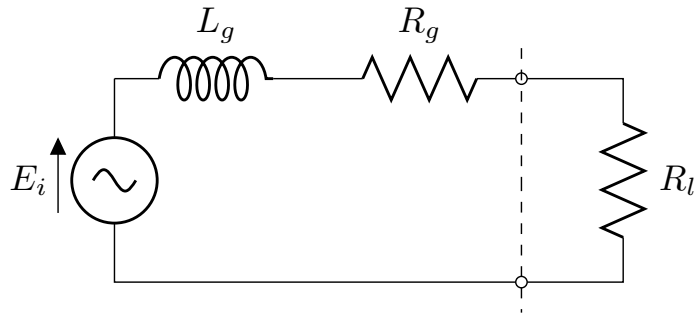

Figure 2.2. One phase equivalent circuit model of the generator connected to an resistive load.

be derived from the generated output power, $P_{el} = IU$, where U is the voltage output of the generator. It should be noted that the damping factor γ is constant if, and only if, P_{el} is proportional to $\dot{x}^2$. To find P_{el}, the generator is often represented as a one phase circuit model, as the one presented in figure 2.1, where E_i is the induced voltage, R_g is the winding resistance, and L_g the generator inductance and R_l is a resistive load connected to the generator. E_i increases linearly with translator speed, and if the circuit would be resistive (no inductance), P_{el} would be proportional to $\dot{x}^2$. However, the inductance will introduce a phase shift between voltage and current, affecting P_{el}. The consequence is a speed dependence of γ unless the inductance is neglectable.

The PTO damping force of the circuit in figure 2.2, assuming resistive external load, full stator overlap and a non salient linear generator, is [36]:

$$F_{PTO}^{el} = \frac{P_{el}}{\dot{x}_t} = \frac{3E_i(\dot{x}_t)^2 R_{tot}}{\dot{x}_t(R_{tot}^2 + X(\dot{x}_t)^2)}, \tag{2.5}$$

where the total resistance is $R_{tot} = R_g + R_l$ and the reactance $X = 2\pi f_{el} L$. The electrical frequency of the generator, f_{el}, is related to the translator speed, $\dot{x}_t$, and the pole width, τ, as: $f_{el} = \frac{\dot{x}_t}{2\tau}$. This model includes copper losses, due to the winding resistance Rg, but neglects iron losses and mechanical losses, thus underestimates the connection line force needed to drive the generator. If Eq. (2.5) is put into Eq. (2.4) to derive a value of γ, it is seen that γ is speed independent only if there is no reactance X. This means that the assumption of a constant γ is only a good approximation if the inductance, L, is low in comparison with the total resistance, and for low speeds.

In order to study WEC behavior and to optimize power absorption, the PTO damping of specific generators has been both modelled and measured. In [51], a lumped circuit analysis, as described above, was used to find a speed dependent PTO damping which was used to simulate WEC absorption. The absorp-

tion for the L1 generator was simulated for 3 levels of external resistive loads; 2.2 Ω, 4.9 Ω and 10 Ω, and compared with offshore experimental data. It was seen that for the load cases of 4.9 Ω and 10 Ω, the speed dependence was low and γ could be approximated as 45 kNs/m and 28 kNs/m respectively. For the 2.2 Ω load, γ had a value of approximately 68 kNs/m for low speeds, but decreasing with increasing speed. The hydromechanical forces on the buoy were calculated using linear potential wave theory, and good agreement was found between the simulations and the experiments, and it was concluded that this modelling could be used with good accuracy to design and optimize wave energy converters in normal operating conditions. The generator damping was simulated and shown as a function of load and generator speed in [52, 53], where γ for resistive external loads was compared with when the generator was connected to a constant DC level. In [22], the output power of the same generator, L1, was measured during offshore operation. In this paper, γ was assumed constant and was calculated from the measured voltage and translator speed. γ was calculated as 38.1 kNs/m, 25.6 kNs/m and 15.7 kNs/m for the load cases of 2.2 Ω, 4.9 Ω and 10 Ω respectively.

It should be noted that for the damping factor derived in [51, 52, 53, 22], both frictional and iron losses were neglected, and that the damping experienced by the WEC was thereby underestimated. As was concluded in [51], the generator damping as expressed in Eq. (2.4) give satisfactory results considering absorbed energy during normal operating conditions. However, it is possible that the differences between F_{PTO}^{el} and F_{PTO}^{mech} will lead to non neglectable differences for the survivability. A more realistic model of the PTO should include the losses. The total power absorbed from the wave can be summarized as:

$$P_{mech} = P_{el} + P_{loss}^{copper} + P_{loss}^{iron} + P_{loss}^{mech}, \tag{2.6}$$

where the losses are separated into copper losses, P_{loss}^{copper}, iron losses, P_{loss}^{iron}, and mechanical, frictional, losses, P_{loss}^{mech}. Copper losses, which are due to internal resistance in the generator and/or cable, can be modelled in the same way as the output power and thus added directly to P_{mech} in Eq. (2.6). P_{el} and P_{loss}^{copper} are most often modelled as RI^2, where R is the winding resistance, and are thus load dependent. Iron losses can be further divided into hysteresis losses, eddy current losses and excess losses. These can be estimated from generator specifications or measured. They are often considered independent of load, but are directly dependent on the electrical frequency, f_{el}, thus dependent on the translator speed. The hysteresis losses are linear dependent on f_{el}, so that $P_{loss}^{hysteres} \propto \dot{x}$. The eddy current losses depend on f_{el}^2 so that $P_{loss}^{eddycurrent} \propto \dot{x}^2$, and the excess losses depend on $f_{el}^{3/2}$ so that $P_{loss}^{excess} \propto \dot{x}^{3/2}$.

Mechanical losses, mainly found in the mechanical piston lead-through and in the guiding wheels on which the translator rolls, depend of the mechanical design of the WEC. The lubricated friction in the piston lead-through can be assumed to depend on the viscosity of the lubricant, which is speed dependent. Pure rolling friction is low and independent of speed. However, since the rubber coated wheels are pretensioned to ensure that the translator is centred, the rubber is deformed and speed dependent visco-elastic friction losses should be expected. The losses will also depend on the pretension.

3. Theory

3.1 Fluid dynamics

3.1.1 Fluid flow

A definition of a fluid is written in [54] as:

Definition: A Newtonian fluid is a substance that may resist shearing (tangential) stress no matter how small only by continuous motion.

This means that a fluid is a material that always deforms if shear stress is applied. Fluids includes liquids, gases and plasmas. Plastic solids may also to some extent be considered as fluids; if the considered time span is long enough, plastic solids, for example glaciers, will flow. By describing the transfer of mass and momentum, the behaviour of fluid flow can be understood. This is described in the continuity equation, Eq. (3.1), and the equation of motion, Eq. (3.2):

$$\frac{\partial \rho}{\partial t} + \nabla \cdot (\rho \bar{u}) = 0, \tag{3.1}$$

$$\frac{\partial \bar{u}}{\partial t} + (\bar{u} \cdot \nabla)\bar{u} = -\frac{1}{\rho}\nabla P + \nu \nabla^2 \bar{u} + \frac{1}{\rho}\bar{f}, \tag{3.2}$$

where $\bar{u}$ is the velocity vector, ρ is the fluid density, P is the pressure field, ν the fluid viscosity and $\bar{f}$ is external force. Incompressible flow is assumed in this formulation.

Navier-Stokes equations, Eq. (3.1) and (3.2), was written down in the 19th century, and has proven great engineering and scientific value. However, not only is there no general analytical solution, but it has not even been proved that smooth solutions always exist for three-dimensional systems of equations. But Navier-Stokes equation can be solved numerically, and is then providing a good description of fluid dynamics, considering both turbulence, viscosity variations and surface tension. In the scientific field of computational fluid dynamics (CFD), time and space are discretised and Navier-Stokes equations are solved numerically, and the accuracy will depend on the resolution of the discretisation as well as further assumptions. CFD modelling, further described in section 3.2, provides a very useful tool with accurate results, but has a high computational cost. Although CFD methods are necessary when nonlinear effects can not be neglected, linear approximations are often valid, and for example in wave power, linear potential flow theory is widely used.

3.1.2 Linear potential flow theory

Linear potential flow theory is a common linearisation, that has proven to give accurate results for point-absorbing wave energy devices during normal operating conditions. Due to it's low computational cost, it is well suited for optimizing wave energy devices to specific sea states and for park simulations, with many separate WECs in operation, as well as for wave-to-wire approaches. For water, the viscosity ν is low, and the viscous term in Eq. (3.2) can be neglected except in regions of large velocity gradients and strong vorticity. Further, if irrotational flow, $\nabla \times \bar{u} = 0$, and constant density are assumed, the velocity $\bar{u}$ can be expressed as the gradient of a scalar velocity potential Φ:

$$\bar{u} = \nabla \Phi. \tag{3.3}$$

For an incompressible fluid, the velocity potential $\Phi(x,y,z,t)$ satisfies Laplace's equation:

$$\nabla^2 \Phi = 0. \tag{3.4}$$

The Bernoulli's equation, relating the velocity potential and the pressure in a fluid, can be derived from Eq. (3.2) by assuming that gravity is the only external force and integration with respect to the space variables:

$$-\frac{P}{\rho} = gz + \frac{\partial \Phi}{\partial t} + \frac{1}{2}|\nabla \Phi|^2 + C(t), \tag{3.5}$$

where irrotational and inviscid flow are assumed. The arbitrary function $C(t)$ can usually be omitted. The term gz is hydrostatic, while the other terms describe the hydrodynamic contribution. If the pressure field is known, the force $\bar{F}$ on a submerged or semi-submerged body can be derived from the velocity potential by integrating over the total pressure P over the wetted surface S:

$$\bar{F} = \int P \hat{n} dS. \tag{3.6}$$

The air-water interface is important in hydromechanical simulations, and is commonly called a "free surface". By assuming that the wave height is low in comparrison with the wave length, a linearised boundary condition for Φ on the free surface can be expressed as [55]:

$$\frac{\partial^2 \Phi}{\partial t^2} + g\frac{\partial \Phi}{\partial z} = -\frac{1}{\rho}\frac{\partial P_a}{\partial t}, \quad z = 0, \tag{3.7}$$

where P_a is the air pressure at the free surface. If P_a is approximated as constant, a linearised theory describes the motion of the water and the surface,

"Linear potential flow theory":

$$\nabla^2\Phi = 0, \quad -h < z < 0, \tag{3.8}$$

$$\frac{\partial^2\Phi}{\partial t^2} + g\frac{\partial\Phi}{\partial z} = 0, \quad z = 0, \tag{3.9}$$

$$\frac{\partial\Phi}{\partial n} = 0, \quad z = -h, \tag{3.10}$$

where a no flow condition, Eq. (3.10), is made for the seabed, at $z = -h$. The normal to any solid surface is n. For a time harmonic surface gravity wave without atmospheric influence, the free surface η is described as:

$$\eta(x,y,t) = Re[Ae^{i(k\bar{x}+\omega t)}], \tag{3.11}$$

where k is the wave number, ω is the angular frequency of the wave, A is the amplitude and $\bar{x} = (x,y)$. For a time harmonic wave, with constant ω, the time t can be extracted [56], so that:

$$\Phi(x,y,z,t) = Re[\phi(x,y,z)e^{i\omega t}]. \tag{3.12}$$

The surface boundary condition of Eq. (3.9) can be further reduced as:

$$g\frac{\partial\phi}{\partial z} - \omega^2\phi = 0. \tag{3.13}$$

Further, a velocity potential ϕ that satisfy Eq. (3.4) and Eq. (3.10) can now be found as:

$$\phi = B\cosh(k(z+h))e^{ikx}, \tag{3.14}$$

where the free surface condition gives B:

$$B = -\frac{igA}{\omega}\frac{1}{\cosh(kh)}. \tag{3.15}$$

The total velocity potential in linear potential flow theory is then written as:

$$\phi = -\frac{igA}{\omega}\frac{\cosh(k(z+h))}{\cosh(kh)}e^{ikx}, \tag{3.16}$$

and since the fluid velocity is the gradient of ϕ, Eq. (3.3), the components of

the velocity field of the water is described by:

$$v_x = \frac{gkA}{\omega}\frac{\cosh(k(z+h))}{\cosh(kh)}e^{ikx}, \tag{3.17}$$

$$v_y = 0, \tag{3.18}$$

$$v_z = \frac{-igkA}{\omega}\frac{\sinh(k(z+h))}{\cosh(kh)}e^{ikx}. \tag{3.19}$$

As can be seen from Eq. (3.17)-(3.19), the water particles will have an elliptic motion, and the radii of the ellipses will decrease with an increasing depth.

A dispersion relation describes the relation between the wave frequency ω and the wave number k, can be derived from Eq. (3.9) as:

$$\omega^2 = gk\tanh(kh) \tag{3.20}$$

for surface gravity waves. Dispersion can be understood as that the propagation speed of waves depends on their wave lengths. Further, the following deep water approximation can be made if $kh \gg 1$:

$$\omega = \sqrt{gk},\ \ kh \gg 1. \tag{3.21}$$

If instead $kh \ll 1$, a shallow water approximation can be made:

$$\omega = k\sqrt{gh},\ \ kh \ll 1. \tag{3.22}$$

The phase speed C of a wave is:

$$C = \frac{\omega}{k} = \sqrt{\frac{g}{k}\tanh kh}. \tag{3.23}$$

For deep and shallow water, C can be approximated as:

$$C = \sqrt{\frac{g}{k}},\ \ kh \gg 1 \tag{3.24}$$

$$C = \sqrt{gh},\ \ kh \ll 1. \tag{3.25}$$

As seen in Eq. (3.24) and (3.25), at deep water, longer waves travel faster than shorter wave. But for shallow water, the speed is proportional to depth instead of wave length.

3.1.3 Energy flow

The total energy transport by a wave, J, is a sum of the potential and kinetic energy, and can be derived as [57]:

$$J = \frac{\rho g^2}{64\pi} T_E H_S^2, \tag{3.26}$$

where T_E is the energy period and H_S is the significant wave height, defined as the mean wave height of the highest third of the waves. The power J transported per meter wave front has the dimension W/m. As can be seen in Eq. (3.17) - (3.19), the wave induced motion of the water decrease with increased depth. Naturally, so does the energy. Depth variation of the energy transport surface gravity waves has been described in [58].

3.2 Computational fluid dynamics

In traditional offshore engineering, CFD methods can be used when nonlinear and highly nonlinear flows are present, such as in highly energetic sea states and extreme waves. Within the field of wave power technology, WECs are designed to maximize power absorption, and in contrast to traditional offshore engineering, the bodies are normally designed to have as large motion and motion response as possible, instead of a small motion response. As a consequence, nonlinear effects can be important for operation during normal operation conditions as well as for survivability in highly energetic sea states [59]. Different CFD methods includes (but are not limited to):

CFD methods

I. Mesh-based Navier-Stokes solvers; where the fully nonlinear Navier-Stokes equations are solved. The finite element method (FEM) or the finite volume method (FVM) are commonly used for the numerical solutions. These methods have a high computational cost but proven to have a high accuracy and are considered as high fidelity models. COMSOL Multiphysics [60] is a common FEM software, while ANSYS Fluent [61] and OpenFOAM [62] uses FVM.

II. Smoothed-particle hydrodynamics (SPH); a mesh free method where the Navier Stokes equations are solved in a domain discretized with an array of particles. High accuracy requires a very large number of particles and very high computational cost. Improvements have however been

achieved in recent years, and with constantly increasing computational power, SPH methods are promising for the future.

In this thesis, mainly the open source software OpenFOAM has been used, where the fully nonlinear Navier Stokes equations are solved with FVM.

3.2.1 Modelling of surface gravity waves with the finite volume method

In FVM, the domain is discretised using control volumes, the desired variable located in the centre of each element. The differential form of the governing equations are then integrated over each control volume. To find the variation of the variable between the control volumes, interpolation profiles are assumed. In FVM, conservation of mass, momentum and energy is guaranteed.

For turbulent flows, the Reynolds decomposition of the fluid velocity can be used [63]. The fluid velocity $\bar{u}$ is decomposed into a mean flow component $\bar{U}$ and fluctuating component $\bar{u}'$; $\bar{u}(\bar{x},t) = \bar{U}(\bar{x}) + \bar{u}'(\bar{x},t)$. The Navier Stokes equations can then be written as the time average Reynolds Average Navier Stokes (RANS) equation:

$$\frac{\partial \bar{U}_i}{\partial t} + \bar{U}\frac{\partial \bar{U}_j \bar{U}_i}{\partial \bar{x}_j} = \bar{f} - \frac{1}{\rho}\frac{\partial p}{\partial \bar{x}_i} + \mu\frac{\partial^2 \bar{U}_i}{\partial \bar{x}_j \partial \bar{x}_j} - \frac{\partial \overline{u_i' u_j'}}{\partial x_j} \tag{3.27}$$

In Eq. (3.27), the fluctuating, turbulent, component $\bar{u}'$, is separated into the last term of the equation. In order to create a closed system of equations, this turbulent last term can be modelled with a turbulence model. Two of the most common turbulence models are the $\kappa - \varepsilon$ model and the $\kappa - \omega$ model, where κ refers to the turbulent kinetic energy, ε refers to dissipation of turbulence kinetic energy and ω to the turbulence frequency.

The presence of the water surface, the interface between the fluid air and the fluid water, can be handled with an interface capturing method. The volume of fluid (VOF) method is a method where a scalar field α is used to track the free surface. In each cell, α describes if the cell contains only air, $\alpha = 0$, only water, $\alpha = 1$, or a mixture. The fluid properties are expressed as:

$$\Phi = \alpha\Phi_{water} + (1-\alpha)\Phi_{air} \tag{3.28}$$

where Φ is a fluid property such as μ or ρ.

The incident wave is implemented as a velocity field and surface elevation at an inlet boundary. Relaxation zones can be used to remove reflected or internally generated wave components adjacent to vertical boundaries [64], where

the solution of velocity, v_c, and surface elevation, tracked by α_c are blended with target solutions, v_t, α_t;

$$v_c = v_c w(\bar{x}) + u_t(1 - w(\bar{x})), \tag{3.29}$$

$$\alpha_c = \alpha_c w(\bar{x}) + \alpha_t(1 - w(\bar{x})), \tag{3.30}$$

where $w(\bar{x}) \in [0, 1]$ is a spatially distributed weighting function.

3.3 Numerical modelling of point absorbing wave energy converters

This section aims to provide a brief literature review of the field of numerical modelling of point-absorbing wave energy converters. Section 3.3 consists of two subsections, the first considering linear aspects, power absorption and optimization, and in the second subsection, fully nonlinear methods are considered. This thesis focus on wave energy converters in extreme waves. In this thesis, extreme waves are defined as waves that are higher than normally expected at the site. An extreme wave can, for example, be a storm surge or a rogue wave, such as the Draupner wave [65], or a tsunami wave. Storm surges and rogue waves are normally deep water waves, their wave lengths are short in comparison with the water depth, while a tsunami wave has a very long wave length and can be considered as a shallow water wave. Section 3.4 in this chapter considers the numerical modelling of tsunami waves.

3.3.1 Linear aspects

During the 1970s, power absorption of point-absorbing WECs was studied by analytical methods, focusing on maximum efficiency [66]. A linearised equation of motion for a general point-absorbing wave energy device moving in heave can be expressed as [16, 67]

$$(m + m_a)\ddot{z} + R_r\dot{z} + Kz = F_{PTO} + F_{ex}, \tag{3.31}$$

where m is the mass of the device and m_a is the hydrodynamic coefficient added mass, z is the vertical coordinate, R_r is the radiation damping, K is stiffness of hydrostatic restoring force, F_{PTO} is the vertical component of the force from the PTO. The excitation force from the waves is F_{ex}. In Eq. (3.31), the force from the water acting on the device has been decomposed into the hydrodynamic coefficients m_a, R_r and F_{ex}. The hydrodynamical coefficients can be solved analytically for simple geometries using linearised approaches [68, 69, 70, 71, 72] or approximate analytical methods [73]. For more complex

geometries, or for studies including nonlinear effects, numerical methods can be used to find hydrodynamical parameters. The boundary equation method (BEM) code WAMIT [74] uses a weakly nonlinear approach to solve for the hydrodynamical parameters in the frequency domain. BEM can also be used with fully nonlinear boundary conditions [75, 76]. By expressing the hydrodynamical parameters as functions of frequency of a monochrome incident wave, it can bee seen that a point-absorbing wave energy device will have a very high energy absorption for it's resonance frequency. In the 1970s, Mei [77], Evans [78] and Newman [79] presented similar reasoning considering the maximum power absorption for a wave energy device moving in one and two degrees of freedom. The floating body's displacement was denoted $z = Re(z_0 e^{-i\omega t})$ and the excitation force $F_{ex} = Re(F_{ex} e^{-i\omega t})$. The hydrodynamic reaction on the body due to the movement of the body itself was denoted $-m_a\ddot{z} - R_r\dot{z}$, and that the PTO force was $F_{PTO} = -m_{PTO}\ddot{z} - \gamma\dot{z}$. By letting m_{tot} be the sum of the added mass, the buoy mass and mass of the moving part of the PTO system, $m_{tot} = m + m_a + m_{PTO}$, the equation of motion in the frequency domain is expressed as:

$$m_{tot}\ddot{z} + (R_r\gamma)\dot{z} + Kz = Re(F_{ex} e^{-i\omega t}), \tag{3.32}$$

where K denotes the static restoring force. The power extracted from the buoy to the generator, $P_{abs} = \gamma\dot{z}^2$, then becomes:

$$P_{abs} = \gamma\dot{z}^2 = \frac{1}{2}\frac{\gamma\omega^2|F_{ex}|^2}{(K - m\omega^2)^2 - (R_r + \gamma)^2\omega^2}. \tag{3.33}$$

From Eq. (3.33), two design criteria were found for maximum absorption; load control: $\gamma = R_r$, that the extracted energy must correspond to the radiation damping, and phase control: $K - (m + m_{PTO})\omega^2 = m_a\omega^2$, that the buoy must be kept in resonance [77]. If those criteria hold, the maximum absorption for a device moving in one degree of freedom will be:

$$P_{max} = \frac{|F_{ex}|^2}{8R_r}. \tag{3.34}$$

Since R_r and F_{ex} are known, they can be inserted into Eq. (3.34) to find that $P_{max} = \frac{1}{2}P_w$, where P_w is the power of the incoming waves passing the buoy. It was also shown that for a device moving in two uncoupled degrees of freedom, $P_{max} = P_w$, all power is extracted. It should be noted that this result is only valid for a device in resonance and with the generator damping matching the radiation damping. To control the phase and load of the optimum device, the future wave must be known. Additionally, an upper limit based on the submerged volume of the device, V, was presented by Budal and Falnes [80]

for harmonic waves, and is commonly refereed to as Budal's upper bound:

$$P_{abs} < P_B = V\frac{\pi\rho hH}{4T}, \tag{3.35}$$

where H is the wave height and T the energy period of the wave. In real applications, the absorbed power will be substantially less than both those upper limits [57]. It should also be noted that absorbed power refers to energy absorbed from the wave by the buoy, which was denoted P_{mech} in section, 2.2.2, and that the power converted to useful energy, for example electricity, will be less: $P_{el} < P_{mech}$.

The equation of motion in Eq. (3.32) can be used as a very fast tool for optimization if the PTO force is linear. A time-domain problem can be Fourier transformed and solved in the frequency domain, and then inverse Fourier transformed back to the time domain [81, 82]. If the PTO is discontinuous or nonlinear, time-domain modelling is necessary. A method developed by Cummins [83], originally for the ship industry, was adapted to the wave energy industry, and the time-domain equation of motion was expressed as [84]:

$$(m+m_a(\infty))\ddot{z}(t)+\int_{-\infty}^{t} L(t-\tau)\ddot{z}(\tau)d\tau = F_{ex}(t)+F_{PTO}, \tag{3.36}$$

where L is the inverse Fourier transform of the impulse response function of the radiation damping:

$$L(t) = \frac{2}{\pi}\int_{0}^{2}\frac{R_r(\omega)}{\omega}\sin(\omega t)d\omega. \tag{3.37}$$

This coupled time-dependent system can also be solved numerically, using a simulation software such as Simulink.

3.3.2 Fully nonlinear modelling approaches

The linear modelling presented in section 3.3.1 provides fast prediction of power absorption, with acceptable agreement during normal operating conditions. However, viscous effects, turbulence, breaking waves and overtopping are effects that can not be neglected during the full life span of a wave energy device. In recent times, CFD methods for wave energy applications has become a rapidly growing area [63]. Much of the development has been performed in the open source software OpenFOAM. RANS-VOF methods, described in section 3.2, have proven accurate even for overturning highly nonlinear flow behaviour of WECs in extreme waves [85]. RANS-VOF can

be used both to identify hydrodynamical parameters or full state dynamics of floating bodies [86, 87], or to model a complete WEC system during an extreme wave event. Several CFD models of WECs have been experimentally verified; in reference [88] the motion of a flap type WEC modelled in OpenFOAM shows good agreement with experiment; in [89], a 2-body point-absorber is modelled in heave motion; in [90] and [91] a point-absorbing WEC with linear-elastic mooring, moving in six degrees of freedom, is modelled showing good agreement with wave tank experiments, and; in reference [92], another point-absorber was modelled both fixed and freely floating. The survivability of the Uppsala University WEC is numerically studied in [93], using a RANS-VOF model verified with experimental data reprinted from [49].

3.4 Modelling of tsunami waves

Tsunami waves refer to surface gravity waves that are caused by large perturbations in the ocean, such as earthquakes, submarine landslides, explosions etc. [94]. Typically in the open ocean, a tsunami has a very long wave length, and can be considered a shallow water wave, propagating with a high speed for long distances. As was seen in Eq. (3.25), the deep water wave speed is related to the depth as $\sqrt{gh}$, so that for an ocean depth of $h = 4000$ m, the tsunami would propagate with a speed of 200 m/s [95]. In the open sea, the amplitude of a tsunami is low, but when it propagates to shallower waters, the wave length decreases and the amplitude increases. Although a tsunami wave in deep sea can be simulated using linear shallow water theory [96], the wave dynamics of a tsunami running up a continental shelf is very complex, and different phenomena may occur, depending on the width and profile of the shelf, the topography of the coast, incident angle of the tsunami and other factors. The tsunami can come in as a fast rising tide with several times the magnitude of a normal tide. It can form a hydraulic jump, a steep wall of water approaching with a speed of several tens of kilometres per hour. It can also form a single or a series of several large breaking waves. The Nihonkai-Chube tsunami, 1983, hit the coast of Japan during mid day, and there were numerous witnesses, photographs and recorded films to study the near-shore behaviour of the tsunami. In [97], a survey was performed presenting near-shore properties of the tsunami. The diagram composed by N. Shuto and reprinted in figure 3.4 shows a large variation in the tsunami behaviour near-shore. In the survey, short-period wave components of about 10 s were confirmed, which evolved to form cnoidal bores, breaking bores, plunging or spilling breakers, standing waves etc. It was pointed out that shallow water theory can not numerically reproduce these wave profiles, and for the Nihonkai-Chube tsunami, N. Shuto concluded that dispersion effects could not be neglected for depths shallower than 50 m.

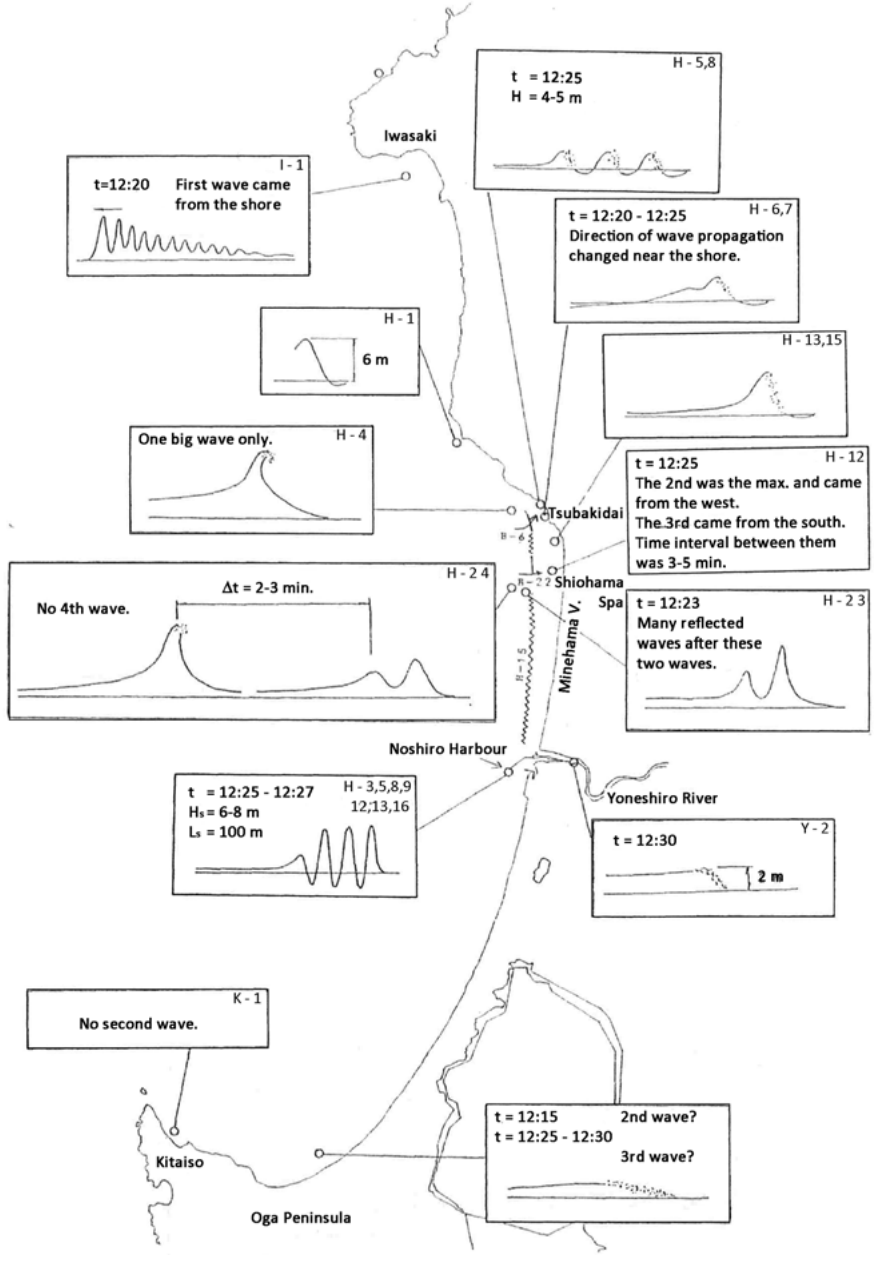

Figure 3.1. Varied near-shore tsunami wave behaviour of the Nihonkai-Chube tsunami, 1985. Reprinted from [97]. Text and box edges have been enhanced to improve readability.

In recent years, numerical simulations using RANS-VOF have been used more frequently to simulate forces from near-shore tsunamis [98, 99]. In a case study by Bricker and Nakayama, OpenFOAM was used to simulate the failure of the Utatsu Highway bridge during the Great East Japan Tsunami in 2011 [100]. The tsunami was recorded on video which showed that it behaved like a fast rising tide, with the surface rising about 1 m/min and a flow speed of about 3 m/s. Both the drag and the lifting force and the overturning momentum was seen to increase slowly, on a time scale of about 10 min, as the inundation increased, until the bridge failed during deep submergence. In [101], the forces on a bridge as it was impacted by a bore type tsunami was simulated with OpenFOAM. The simulations showed good agreement with scaled wavetank experiments for both the initial impacting force and the remaining force as the bridge got submerged. Numerical simulations of tsunami waves are often done as solitary waves or dam-break approximations [102, 103]. OpenFOAM was used in [102] to study bore profiles, flow velocities, pressure, run-up and forces on coastal structures from a dam-break tsunami approximation. Dry bed and wet bed conditions were compared, showing non-neglectable differences. The survivability of an oscillating wave surge converter struck by tsunami was studied in [104]. Linear shallow water theory was used and it was seen that the pressure jump across the plate from a tsunami with an amplitude of 4 m and period of 10 min was significantly smaller than typical swells during normal operating conditions. The authors do however also point out that nonlinear effects can not be neglected at the current depth of 10 m, and that the linear theory underestimates the force significantly.

Part II:
Modelling of forces on a point-absorbing wave energy converter

4. Methodology

In this thesis, the survivability of a WEC in harsh operating conditions and in tsunami waves has been studied. A fully nonlinear RANS-VOF numerical model has been developed and verified with physical wave tank experiments. It has then been used to study motion and forces on the WEC in extreme waves; high regular waves and during tsunami events, and how the WEC behaviour is influenced by different generator parameters, such as generator damping, friction and length of the connection line.

Since the forces and the motion of the WEC are highly dependent on the generator behaviour, the generator damping of two different full scale linear generators has been studied during onshore experiments. The RANS-VOF model was then used to study the consequences of the discrepancies between the experimentally measured generator behaviour and an assumed linear behaviour.

The RANS-VOF model is described in section 4.1 and the experiments on the full scale generators are described in section 4.2.

4.1 The numerical model

The fully nonlinear model has been developed in the open-source software OpenFOAM v2.4.0. The Scotch method has been used to decompose the simulation jobs which were then run on Xeon E5-2630 V4 processors running at 2.2 GHz.

4.1.1 Governing equations

The Reynolds Averaged Navier-Stokes equations are closed with an RNG $\kappa - \varepsilon$ turbulence model. The two-phase Navier-Stokes solver interDyMFoam is used, where the equations for the air and the water are written assuming a single fluid mixture:

$$\nabla \cdot \bar{u} = 0, \tag{4.1}$$

$$\frac{\partial}{\partial t}(\rho \bar{u}) + \nabla \cdot (\rho(\bar{u} - \bar{u}_g)\bar{u}) = -\nabla p + \nabla \cdot \bar{S} + \rho \bar{f}_b, \tag{4.2}$$

where $\bar{u}$ is the fluid velocity and $\bar{u}_g$ is the grid velocity, ρ is the mixture density and p is the pressure. $\bar{S} = 2\mu\bar{D}$ is the viscous stress tensor where μ is the

mixture viscosity, $\bar{D}$ is the strain tensor and f_b is the force from a rigid body. The volume of fluid (VOF) method is using a scalar field α to track the two fluids and the surface boundary, $\alpha = 1$ denotes water and $\alpha = 0$ denotes air, and values in between are a mixture. The transport equation for α is:

$$\frac{\partial \alpha}{\partial t} + \nabla(\alpha(\bar{v} - \bar{v_g}). \tag{4.3}$$

4.1.2 Fluid-rigid body interaction

The buoy of the WEC is modelled as a floating rigid body in a numerical wave tank, moving in six degrees of freedom, moored to a fixed position; either at the seabed or at the top of a generator hull. The linear generator is modelled as a restraining force in the mooring line, $F_{line}\hat{r}$ (see figure 4.1 a). The vector $\bar{r} = r\hat{r}$ is the vector pointing from the buoy position to the anchoring position. The native OpenFOAM solver sixDoFRigidBodyMotion integrates the pressure force $p\hat{n}$ and the shear force vector τ acting on the buoys surface S to find the resulting force and force moment acting on the buoy:

$$\bar{F} = \iint_S (p\hat{n} + \tau)dS + F_{line}\hat{r}, \tag{4.4}$$

$$\bar{M} = \iint_S (\bar{r_{cs}} \times ((p\hat{n} + \tau)))dS, \tag{4.5}$$

where $\bar{r}_{cs}$ denotes the vector from the centre of mass to the centre of each surface panel. The mesh deforms with the motion of the buoy.

The restraining force from the generator is described as a function, calculated in each time iteration. It is a sum of the gravity force on the translator $F_{m_t g} = m_t g$, the electromagnetic damping in the generator, F_{PTO}, frictional loss, F_{fric} and endstop forces when the stroke length is exceeded. F_{PTO} and F_{fric} are directed in the opposite direction of the translator movement. As seen in figure 4.1 b), the translator-stator overlap is not full during the whole stroke length, and F_{PTO} must be multiplied with A^c_{frac}, where the factor A_{frac} is the fraction of the translator-stator overlap and the stator area, and c is a factor. When the translator hits the upper endstop spring, a restraining endstop spring force is added; $F_s = \kappa_s(r - r_{rest} - l^{up}_{free})$, where r_{rest} is the length of r at still water and the translator stands in the middle position. l^{up}_{free} is the free stroke length, seen in figure 4.1 b). If the endstop spring gets fully compressed, a second endstop force is added, corresponding to the elasticity of the connection line; $F_{endstop} = \kappa_{line}(r - r_{rest} - l^{up}_{total})$, where l^{up}_{total} is the total stroke length, seen in figure 4.1 b). The Heaviside functions δ_{free} and δ_{total} define when

the endstop spring is hit and when it is fully compressed, and depends on the length of the the vector $\bar{r}$ as:

$$\delta_{free}/\delta_{total} = \begin{cases} 1, & r > r_{rest} + l^{up}_{free}/l^{up}_{total} \\ 0, & \text{otherwise.} \end{cases} \tag{4.6}$$

When the translator stands on the bottom of the WEC, the line is slack and F_{line} is set to zero using the Heaviside function δ_{down}. The total restraining force is described by:

$$\bar{F}_{line} = \delta_{down}(-m_t g \mp F_{PTO} A^c_{frac} - \kappa r \mp F_{fric} - F_s \delta_{free} - F_{endstop}\delta_{total})\hat{r}. \tag{4.7}$$

If F_{line} becomes a positive number, the line would slack and F_{line} is set to zero. Since the translator position is derived from the length of $\bar{r}$, the position is not known when the line slacks.

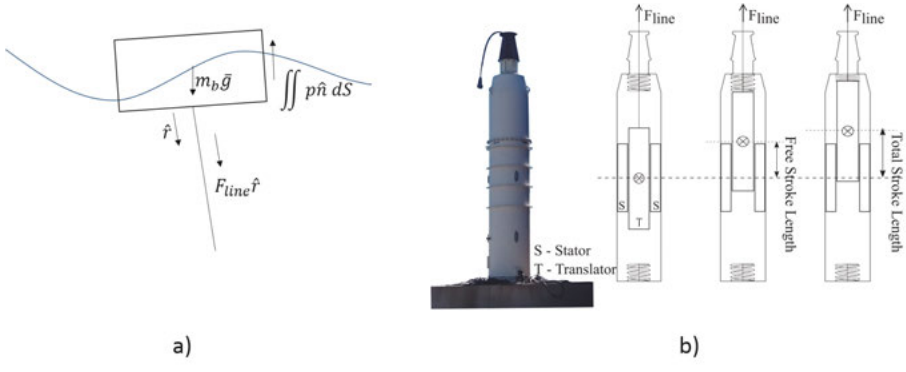

Figure 4.1. (**a**) The WEC is modelled as a floating buoy, restrained by a force in the connection line. The force is directed along a vector pointing at the fixed anchoring position. (**b**) The generator has a limited stroke length. It can also be seen that the translator-stator overlap is not full during the whole stroke length.

4.1.3 The numerical wave tank

The simulation domain, seen in figure 4.2 is 300 m long, 100 m high and has a width of 60 m. This is the domain used in paper I, II and III, and the water depth is 50 m. In paper IV, V, VI and VIII, the water depth was 26 m to resemble the conditions at the Lysekil test site. In these papers, the domain height was 75 m. According to the mesh resolution study performed and presented in paper IV, each background mesh element had a side length of 2.5 m, which was refined to 0.625 m in a 25 m high box around the water surface. In the vicinity of the buoy, each mesh element was further refined

to 0.078 m. Two different buoy geometries have been modelled; a cylinder buoy, seen in figure 4.3 (a), and a cylinder with a moonpool, seen in figure 4.3 (b). The buoys have the same height, volume and cross sectional area. They were chosen to resemble the 1:20 scaled buoys used in the physical wave tank experiments presented in [49], which was also the physical experimental data that was used in paper I to validate the model. However, all the simulations are run in full scale in this thesis for engineering usability.

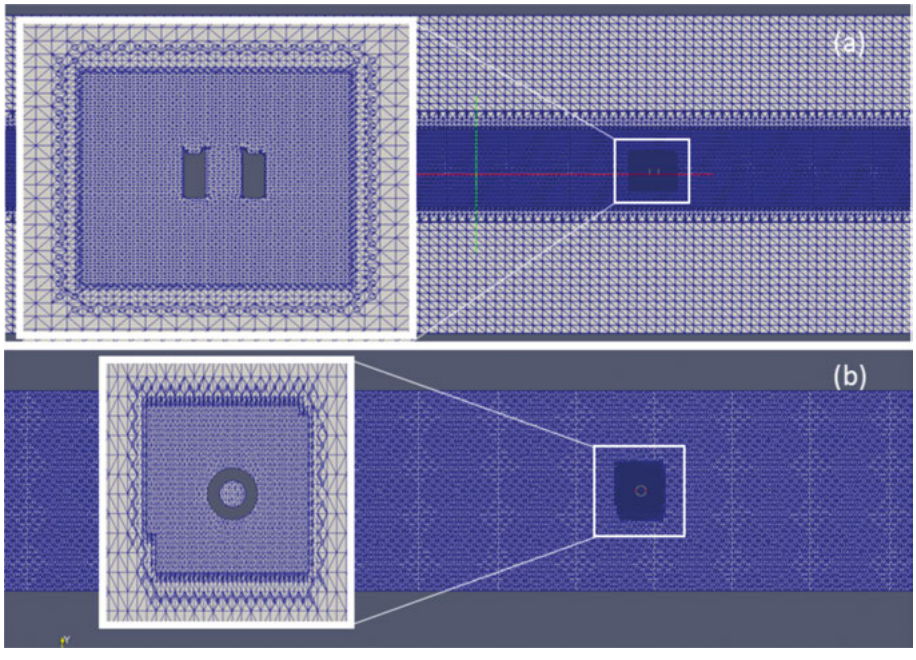

Figure 4.2. (**a**) A 2D section view of the simulation domain seen from the side. A cylindrical buoy with a moonpool is seen here. (**b**) A 2D section view of the simulation domain seen from the top.

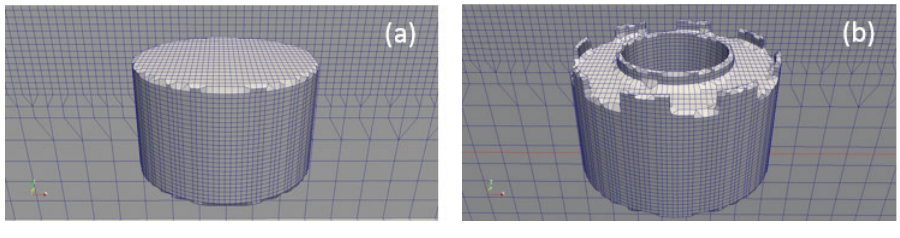

Figure 4.3. (**a**) The modelled cylindrical buoy. (**b**) The cylindrical buoy with a moonpool.

4.1.4 Incident waves

The incident waves are implemented using the OpenFOAM library waves2foam [64], in which the fluid velocity, the surface elevation, and the surface normal pressure gradient are defined as algebraic expressions at the inlet boundary, and relaxation zones are used to eliminate reflections. In this thesis, both regular waves and regular waves with an embedded extreme wave have been modelled, and compared to three kinds of tsunami wave simulations.

Stokes 5th waves

The Stokes wave generator of the waves2foam library was used to generate 5th ordered waves to implement the regular waves. In paper I and II, an event with an extreme wave embedded in regular waves was modelled in a physical wave tank. Frequency analysis of the measured surface elevation was performed, and the four most significant wave components were superimposed to reproduce the wave profile.

Tsunami wave I: Solitary wave

The first order solitary wave of waves2foam is simulated where the equation for the surface elevation of a wave propagating in the x-direction is:

$$\eta(x,t) = H\text{sech}^2(\sqrt{\frac{3H}{4h^3}}(Ct-x)), \tag{4.8}$$

where H is the wave height and the wave celerity is $C = \sqrt{g(H+h)}$. This simulation strategy was used in paper IV.

Tsunami wave II: High speed incident current

A tsunami wave profile with high velocity in the whole water column was simulated by setting a constant inlet velocity at the inlet boundary in a wavetank with no initial water velocity. As the simulation started, the incident water flow forced the water to form a wave profile with one leading high wave, followed by a second slightly lower wave. The wave theory "potential current" from the library waves2foam was used, where a constant inflow of 6.3 m/s in the x-direction was set at the inlet boundary. This simulation strategy was used in paper IV.

Tsunami wave III: Dam-break approach

A dam-break simulation is a common approximation of a near shore or on shore propagating tsunami [102, 105]. The simulation domain was elongated to 600 m, and a water volume with a length of 400 m, a width of 60 m and a height of 12 m was initially placed on top of a constant water surface. The water volume was released when the simulation started. This simulation strategy was used in paper IV, V and VI.

4.2 Physical experiments

The WEC behaviour is highly dependent on the force in the connection line, F_{line}. A large part of F_{line} is the damping force from the generator, F_{PTO}, which is commonly assumed to behave like a linear damper, $F_{PTO} = \gamma \dot{x}$. The damping factor γ is commonly assumed to be constant, which, as discussed in section 2.2.2, is a good approximation if the inductance is low compared to the resistance, and the translator speed is low. The expected F_{PTO}^{el} can be approximated from Eq. 2.5, but mechanical and electrical losses will be neglected. Onshore testing of a full scale generator prototype is necessary to predict and analyse its offshore behaviour. In this thesis, F_{line} for two different full scale generator prototypes has been experimentally measured at resistive load. The magnetic material in the translator of the first measured generator was Nd-Fe-B, while the magnetic material for the second measured generator was ferrite.

4.2.1 Experiment on a Nd-Fe-B generator

The Nd-Fe-B generator prototype, refereed to as "L10" in the Lysekil project, is seen fully mounted in figure 4.4 (a). The Nd-Fe-B permanent magnets of the translator, figure 4.4 (b), were surface mounted. In figure 4.4 (c), the stator is seen before the generator was assembled. Four rows of guiding wheels on which the translator is rolling can be seen. The winding configuration is described in [106]. The generator parameters and the experimental setup is described in detail in paper VII.

The experiment was performed with the generator fully assembled. A Liebherr mobile crane was used to lift the translator until the upper endstop spring was hit, and then lowering it again, with the same speed. This was repeated for a high and low lift speed, and for five resistive load cases. Care was taken

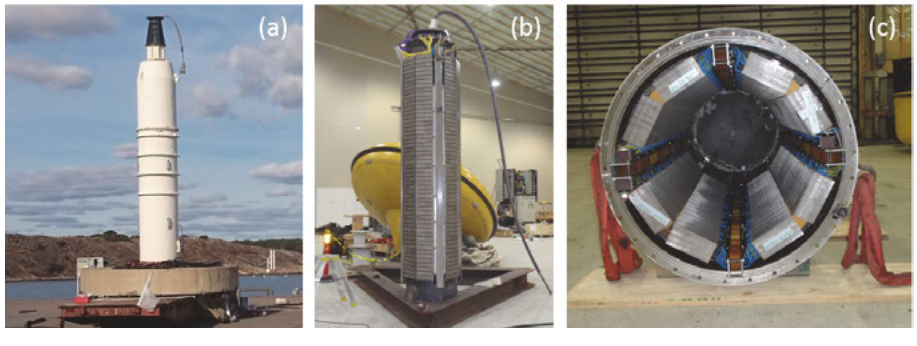

Figure 4.4. (**a**) The fully assembled linear generator. (**b**) The translator with surface mounted Nd-Fe-B permanent magnets. (**c**) The stator is mounted on the inside of the generator hull. Four rows on guiding wheels, light brown, are seen, on which the translator rolls when the generator is assembled.

to keep the speed constant to the greatest extent possible, considering that a crane is an imprecise tool. A force sensor was connected between the translator and the crane, measuring F_{line} for the total stroke length. The translator motion was calculated from the generator output voltage, knowing that the distance between two zero-crossings in the voltage signal corresponds to one pole-width of the linear generator. In paper VII, the measured F_{line} and the derived F_{PTO}^{mech} was plotted as a function of translator position for the full stroke length, comparing the five load cases and the high and low speed. For the low constant speed of 0.1 m/s, γ was derived and plotted as a function of stroke length.

4.2.2 Experiment on a ferrite generator

In the experiment presented in paper VIII, the load and speed dependence of the generator damping was studied for a Ferrite generator. Ferrite magnets have weaker magnetic fields than Nd-Fe-B magnets, which is compensated with more magnetic material. and the translator is built with buried magnets instead of surface mounted. The argument for using ferrite instead of Nd-Fe-B is economical [35], but it should be noticed that the ferrite translator is heavier and that the generator inductance and saliency increase.

Figure 4.5. (**a**) The ferrite generator in front of the crane used in the experiment. The generator hull was mounted on a concrete foundation during the experiment. (**b**) The force sensor was attached between the translator and the crane. The translator is standing on the lower enstop spring in this figure.

A 220t Liebherr crane was used to lift the translator while line force, position and acceleration were measured, as well as voltage and current. This was repeated for twelve speeds and for each of the seven resistive load cases. Figure 4.5 (a) shows the crane and the ferrite generator, and in figure 4.5 (b), the force sensor is seen mounted between the translator and the crane. The experiment

was performed before the top structure of the generator hull was welded on place, which allowed the translator to be lifted higher to study the decreasing F_{PTO} at partial translator-stator overlap. However, the mechanical loss in the piston lead-through was thereby not included in the measurements.

In paper VIII, the measured F_{PTO}^{mech} and F_{PTO}^{el} were compared for translator speeds up to 0.6 m/s, which was the highest speed that could be achieved with the crane, considering the short distance available for acceleration. Corresponding $\gamma(\dot{x})$ values were derived, and the RANS-VOF model presented in section 4.1 was used to analyse the consequences of the difference between F_{PTO}^{mech} and F_{PTO}^{el} for survivability of a WEC. This was also compared with a case were the PTO was assumed to behave like a linear damper, $F_{PTO}^{linear} = \gamma\dot{x}$, where γ was set constant.

Measurements from this experiment was also analysed in paper IX, where P_{el} was studied at partial translator-stator overlap.

5. Results and discussion

This chapter is based on the results presented in the papers included in this thesis, and it is comprised of four sections. In section 5.1, the RANS-VOF model described in section 4.1 is validated with data from physical wave tank experiments. In section 5.2, the RANS-VOF model is used to study different aspects influencing the survivability of a point-absorbing WEC in harsh operating conditions. Section 5.3 considers WEC survivability in tsunami waves. In section 5.1, 5.2 and 5.3, the PTO damping is modelled as a linear damper and/or a constant friction, while in section 5.4, the consequences of a nonlinear PTO system for the WEC behaviour are considered.

5.1 Validation of the RANS-VOF model

The RANS-VOF model built in OpenFOAM was validated in paper I, where the force in the connection line and the buoy motion was compared with physical wave tank data, showing good agreement. The experiment is described in detail in [49]. An extreme wave event, embedded in regular waves, was produced in the COAST Laboratory Ocean Basin at Plymouth University, UK.

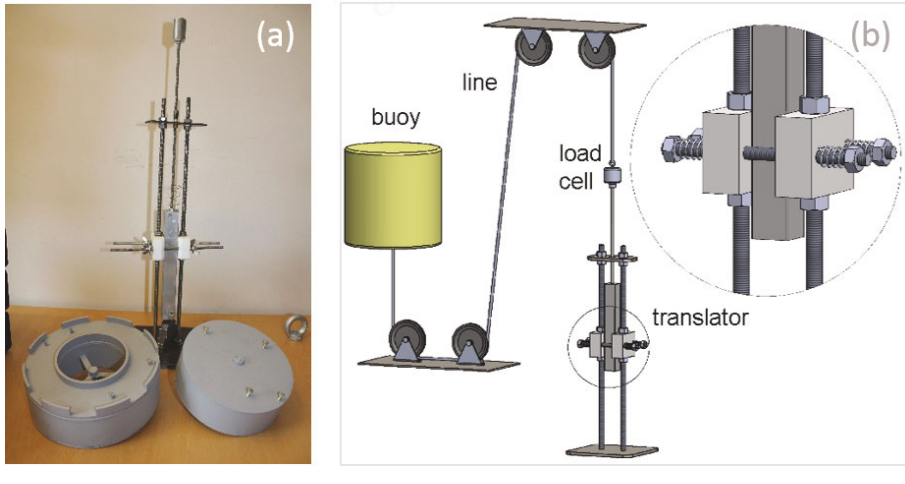

Figure 5.1. (**a**) The 1:20 scale physical model of the PTO system and the two tested buoys. (**b**) The buoy in the wave tank was attached to the PTO via a pulley system and an 8 m long polymer line.

The wave tank measured 35 m $\times$ 15.5 m and the water depth was set to 2.5 m. A 1:20 scale model of a WEC was built, seen in figure 5.1. The position of the buoy was measured with an optical Qualisys system, consisting of five cameras outside the basin and four infrared markers attached to the buoy. The PTO was simplified as frictional damping, which was applied using adjustable Teflon blocks that were pressing on either side of the translator.

5.1.1 Line force and peak line forces

The OpenFOAM model showed good agreement with the physical wave tank results. In figure 5.2, the modelled force in the connection line is compared with the measured force. An incident wave with a wave height of 5.7 m and a period time of 10 s was modelled, and at $t = 105$ s, an extreme wave event was embedded. The physical wave tank event was run for 500 s, while 150 flow seconds were simulated in the OpenFOAM model. Figure 5.2 shows the result for the cylinder with moonpool, comparing no applied damping with an applied friction of 59 kN (1:1 scale), and in figure 5.3, the peak line force of each wave peak from figure 5.2 has been plotted as a function of wave height of each corresponding wave peak. One challenge in numerical wave tank modelling is to implement the same incident wave as in a physical wave tank, or in the ocean. For validation studies, this can, to some extent, be com-

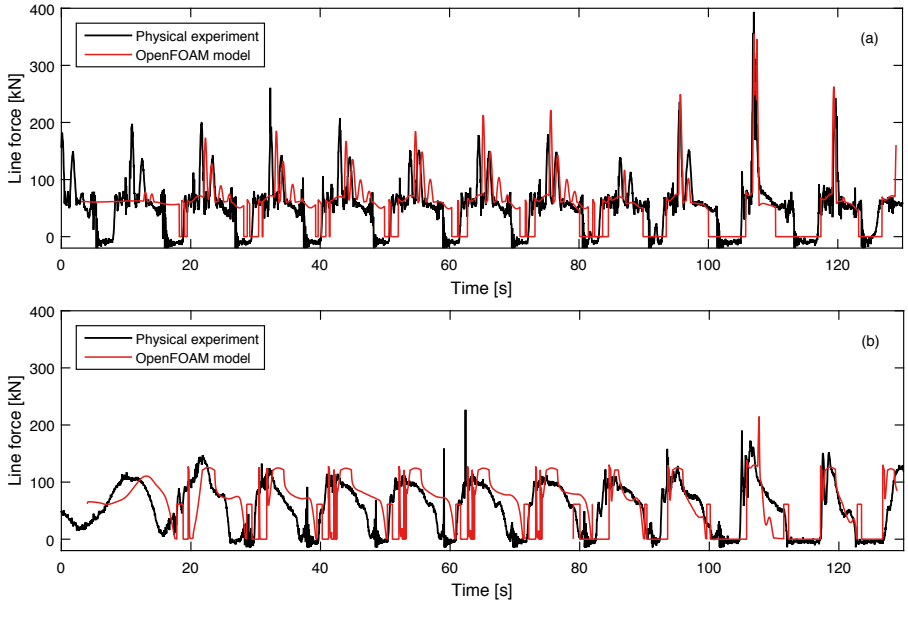

Figure 5.2. The measured line force in the physical wave tank compared with the OpenFOAM model. The cylinder with moonpool was used as a float. (**a**) No damping was applied. (**b**) Frictional damping of 59 kN was applied.

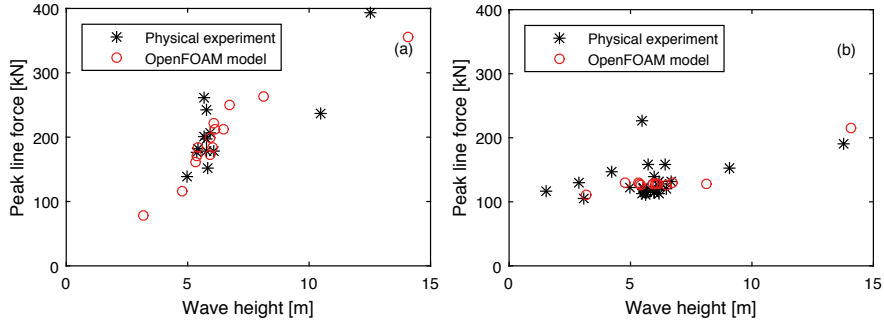

Figure 5.3. The peak forces of figure 5.2 plotted as function of wave height of corresponding wave peak. (**a**) No damping was applied. (**b**) Frictional damping of 59 kN was applied.

pensated for by plotting each peak line force as a function of corresponding wave height, although it should be noted that a WEC response depends on load history and structural dynamics as well as surface elevation [107]. In paper I, this comparison was done for both buoy geometries. For the cylinder buoy, no applied damping and 59 kN frictional damping were studied. For the cylinder with moonpool, four levels of damping were studied; no damping, 18 kN, 59 kN and 83 kN of applied frictional damping. Peak forces from the OpenFOAM model were compared with both physical wave tank data and peak forces modelled in a linear model and a RANS-VOF model built in ANSYS Fluent. Good agreement was found between the physical wave tank data and both RANS-VOF models. As can be seen in figure 5.3, the peak line forces of the OpenFOAM model compared with the physical wave tank data show very good agreement. In paper I, the physical experiments were also compared with results from a linear model, were differences up to several hundred percent could be seen. Further, it was also interesting to find that the linear model did actually show acceptable agreement when no damping was applied, and for the cylinder buoy, but that the model performance was poor when damping was applied, or for the buoy geometry with the moonpool. It was concluded that if a numerical model is intended to study the influence of a specific parameter, such as damping or buoy geometry, the model should be validated with physical experiments including this parameter.

5.1.2 Mesh refinement

The OpenFOAM model was validated in paper I, and the same settings and mesh were used in paper II and III. In paper IV - VI and VIII, the depth of the numerical wave tank was set to 26 m, to resemble the depth at the Lysekil test site. To ensure the validity of the new mesh, a new mesh resolution study was performed and presented in paper IV, and is seen in figure 5.4. The deviation of the line force from the result of the finest mesh is seen in figure 5.4 (b). It

is clear that the line force converged, and it was assumed that the finer meshes were fine enough. According to this, the mesh consisting of 1988 000 hexahedral mesh elements, highlighted by a red marker in figure 5.4, was chosen.

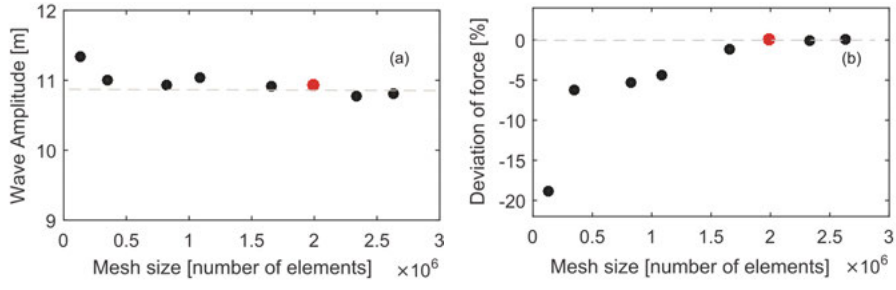

Figure 5.4. (**a**) The wave amplitude presented as a function of number of mesh elements. (**b**) The deviation of line force from the line force of the finest mesh. The magnitude of the line force is converging.

5.2 Connection line force of a WEC in high regular waves

The peak force when the WEC exceeds its stroke length is the main focus in this thesis, and different aspects influencing the endstop forces are studied in paper I-VIII.

5.2.1 The influence of buoy geometry

In paper I-III, two buoy geometries were modelled, a cylinder and a cylinder with moonpool. In the physical wave tank experiment that was used for model validation, described in section 5.1, the buoys had the same cross sectional area, height and volume, but the cylinder with moonpool buoy had a higher mass. In paper II, the line force was normalized with buoyancy to allow comparison. In the physical wave tank, two irregular wave sets based on a JONSWAP spectrum were run to obtain the system's response in realistic operating conditions. The significant wave height for the two irregular waves was 7.2 m and 7.4 m, the maximal wave height 12.9 m and 11.7 m, and the energy period 13.4 s and 14.0 s, respectively. In figure 5.5, the Gaussian distribution of the normalized line force for the two buoys in irregular waves is presented. It is seen that the cylinder buoy has a higher risk for higher peak forces, but there is a large spread among the force measurements.

In paper III, the validated RANS-VOF model was used to model the same

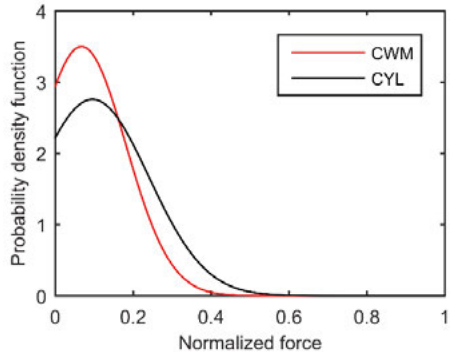

Figure 5.5. Gaussian distribution of the peak forces in the physical wave tank experiment. The cylinder buoy (CYL) is compared with the cylinder with moonpool (CWM). The force is normalized with buoyancy.

two buoy geometries, using the same mass for both buoys. The buoys were modelled in the same waves for three levels of PTO damping, and the average peak force for each buoy was calculated and is presented in table 5.1. The force difference between the buoys, also presented in table 5.1, was calculated as $\text{Diff}(F_{peak}) = (F_{CYL} - F_{CWM})/F_{CYL}$. The peak forces on the cylinder buoy was higher than on the cylinder with moonpool, which is likely a consequence of the lower added mass [108, 109]. It should be noted that the decreased line force also will decrease the possible absorbed energy that can be converted to electricity, which, however, has not been studied in this thesis.

Table 5.1. *Average Peak Force*

PTO damping	**F*peak* CWM**	**F*peak* CYL**	**F*peak* difference**
no damping	151.5 kN	172.5 kN	12 %
10 kNs/m	144.9 kN	169.0 kN	14 %
30 kNs/m	100.8 kN	110.9 kN	9 %

5.2.2 The influence of overtopping waves

In paper III, the WEC was modelled in waves of increasing wave height, and peak line forces from waves that did not overtop the buoy were compared with peak forces when overtopping occurred. This was repeated for two buoy geometries and three levels of damping, the average peak forces are presented in table 5.1. In figure 5.6, the peak forces are plotted as a function of wave amplitude for the cylinder with moonpool buoy, comparing a damping of 10 kNs/m, figure 5.6 (a), with 30 kNs/m, figure 5.6 (b). In the modelled WEC, the length of the endstop spring was set long enough for the endstop spring to never be fully compressed, and an endstop hit was defined as when the

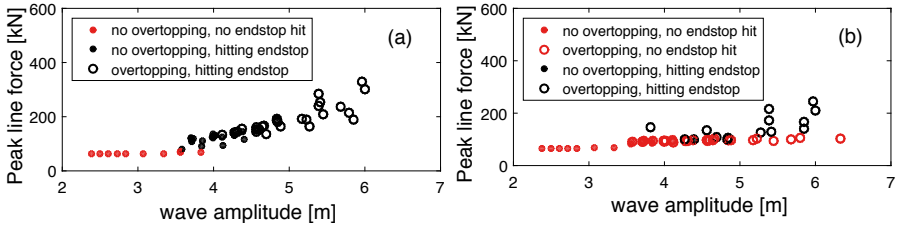

Figure 5.6. The peak line forces of a WEC as a function of wave amplitude. Overtopping waves and when the translator hits the endstop spring are marked. A cylinder with moonpool was modelled as buoy. (**a**) A PTO damping of 10 kNs/m was applied. (**b**) A PTO damping of 30 kNs/m was applied.

endstop spring was hit. Endstop hits are marked in black in figure 5.6, while red markers are used for when the endstop spring was not hit. Overtopping waves are marked with rings, and not overtopping waves are marked as filled dots. By separating overtopping waves and endstop hits, it was seen that if the endstop was hit, the peak force was not influenced by overtopping. This is seen in figure 5.6 (a), the peak forces of the endstop hits, black markers, increase equally with increased wave amplitude, regardless if overtopping occured or not. But when the generator damping was increased, it was seen that if the damping was high enough to prevent the translator from hitting the endstop spring, red markers in figure 5.6, the buoy was overtopped for lower waves and the peak forces were limited even for higher wave amplitudes.

5.2.3 The influence of linear PTO damping

As can be understood from Eq. (2.2), an increased generator damping will increase the force in the connection line if the translator speed is constant. This was also measured in paper VII, and as is seen in figure 2 and figure 3 in paper VII, a higher PTO damping (lower applied resistive load) resulted in a higher line force during the whole stroke length of the machine. However, during offshore operation, the speed of the translator will not be constant, but dependent of the energy in the waves as well as all forces from the generator; PTO damping, friction, gravity and endstop forces. Increasing those forces may decrease the speed of the translator, which may decrease the peak forces during offshore operation. The hydrodynamic force of the wave is dependent on the phase shift between the buoy position and the incident wave, a fact utilized for increasing the energy absorption of a WEC by active control. However, even without active control, passive forces will increase the phase shift between the buoy and the wave, which may increase the peak forces.

In paper VI, the peak forces as a function of wave height were studied for eight levels of linear PTO damping, from generator damping coefficient $\gamma = 0$ to $\gamma = 140$ kNs/m. In figure 5.7, the peak forces are plotted as a func-

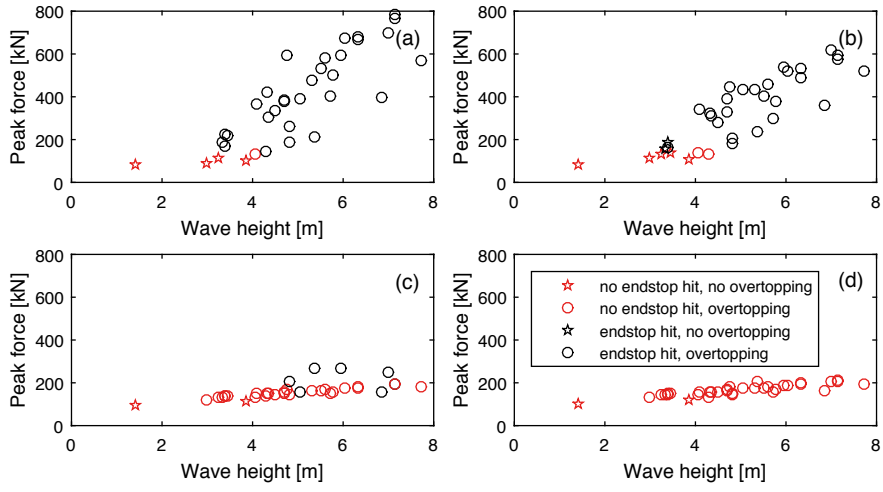

Figure 5.7. Peak forces in the connection line. An endstop hit is defined as a fully compressed endstop spring. (**a**) No generator damping. (**b**) $\gamma = 40$ kNs/m. (**c**) $\gamma = 80$ kNs/m. (**d**) $\gamma = 120$ kNs/m.

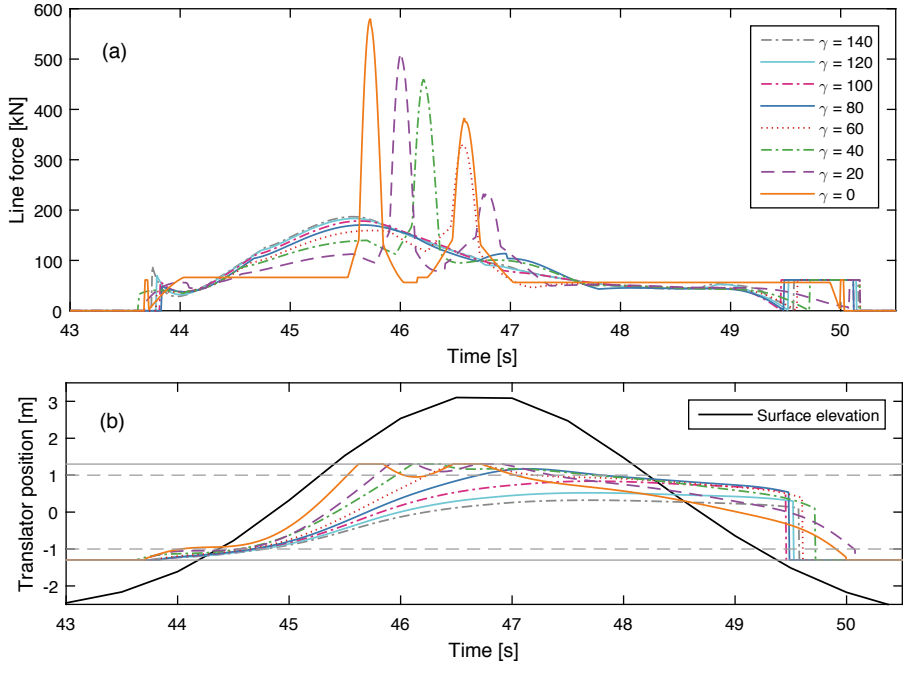

Figure 5.8. A WEC in a regular wave event of 70 s was modelled. This figure shows a zoom of a wave peak, comparing eight levels of linear PTO damping. (**a**) The force in the connection line. The peak forces of the endstop hits decrease with increased PTO damping. (**b**) The translator position. The horizontal dashed lines mark the free stroke length, and the solid lines mark the total stroke length.

tion of wave height, no damping, $\gamma = 40$ kNs/m, $\gamma = 80$ kNs/m and $\gamma = 120$ kNs/m. The same strategy as in paper III was followed, but the WEC parameters were chosen to resemble a WEC at the Lysekil research site, and the studied wave heights were chosen to resemble harsh operating conditions at the site. The decreased PTO damping during partial translator-stator overlap was also included in the model. As can be seen in figure 5.7, most of the waves overtopped the buoy, and the endstop spring got fully compressed for the higher waves. It was seen that when the endstop spring was fully compressed, the magnitude of the peak forces increased approximately linear with wave height. It was also seen that increased PTO damping decreased the peak forces. For the studied WEC parameters and in the studied sea state, a linear PTO damping of $\gamma = 100$ kNs/m was enough to prevent endstop hits. Further increased PTO damping did not further reduce the peak forces, but instead they increased, as predicted by Eq. (2.2). When the endstop is not hit, the highest force in the connection line depends on the strength of the generator; since a higher PTO damping means a stronger generator, the line force increases. However, this increased line force is desired as it can be converted to electricity, in contrast to the damaging force of the endstop hit. This is also seen in figure 5.8 (a), where the force in the connection line is seen for one wave peak, comparing different levels of PTO damping. The translator position is shown in figure 5.8 (b), where the free stroke length is marked by the horizontal dashed lines, and the total stroke length is marked by solid lines. The surface elevation is measured at a wave gauge right above the generator position. If the total stroke length is reached, which can be seen in figure 5.8 (b), the endstop spring is fully compressed and it is seen that increased PTO damping decreased the peak force. For this particular wave peak, a PTO damping of 80 kNs/m or higher was strong enough to keep the translator from fully compressing the upper endstop spring, and avoid the high damaging peak force. Further increased PTO damping increased the line force, but the force magnitude was significantly lower than if the total stroke length was exceeded.

5.2.4 The influence of friction

In paper VI, the influence of friction was studied as well, for both regular waves and tsunami waves. In this paper, friction was assumed to be a constant force, $F_{fric} = constant$, however, it can be noted that frictional losses may be speed dependent. In figure 5.9, the endstop force is seen for one specific regular wave peak, comparing different levels of friction. The PTO damping was set to $\gamma = 40$ kNs/m, while the friction was varied from no friction to F_{fric} = 35 kN. For this regular wave peak, it is clear that an increased friction decreased the peak force. The same pattern was seen for all regular wave peaks. However, both for the tsunami waves and for wave peaks that were higher than there previous wave peaks, as when the energy in the sea state increased, this pattern was not seen, which will be further studied in section 5.3.2.

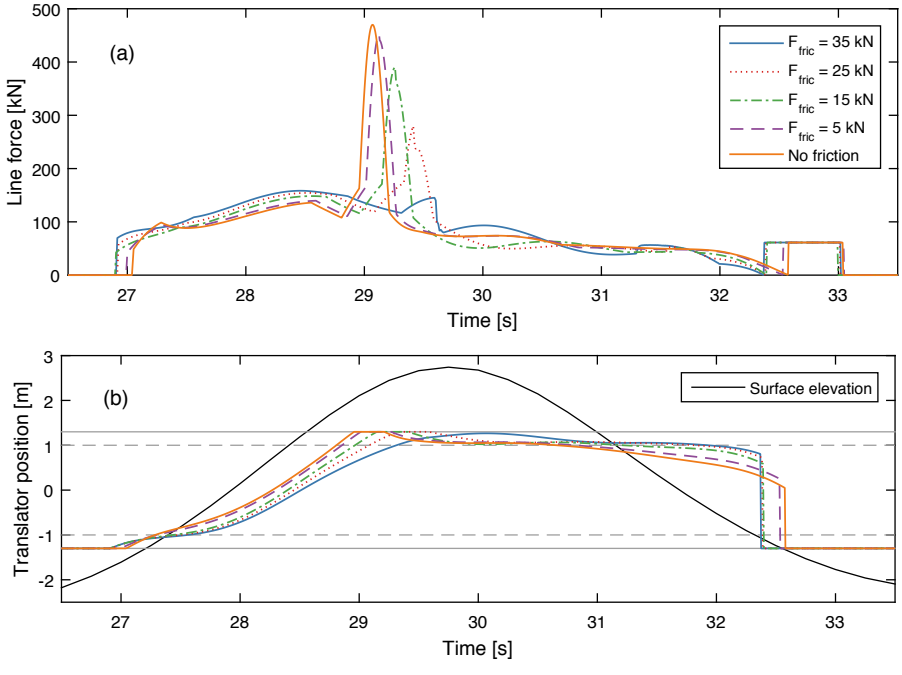

Figure 5.9. The influence of friction on is seen for one wave peak. (**a**) The force in the connection line. The peak forces of the endstop hits decrease with increased friction for this specific wave peak. (**b**) The translator position. The horizontal dashed lines mark the free stroke length, and the solid lines mark the total stroke length.

5.3 WEC behaviour in tsunami waves

5.3.1 Numerical modelling of tsunami waves

At deep water, a tsunami wave can be modelled using linear shallow water theory. But as discussed in section 3.4, when the tsunami wave propagates up on the continental shelf, the wave dynamics is very complex and non linear behaviour must be considered. Different wave phenomena can occur, and to the authors knowledge, there is not yet consensus on which modelling approach is the best. In paper IV, three numerical tsunami modelling approaches were compared; a solitay wave, a high speed incident current and a dam-break approach. A regular wave was also simulated as a Stokes 5th wave. A numerical wave tank with a depth of 26 m was used, and the simulations were run both with and without a WEC.

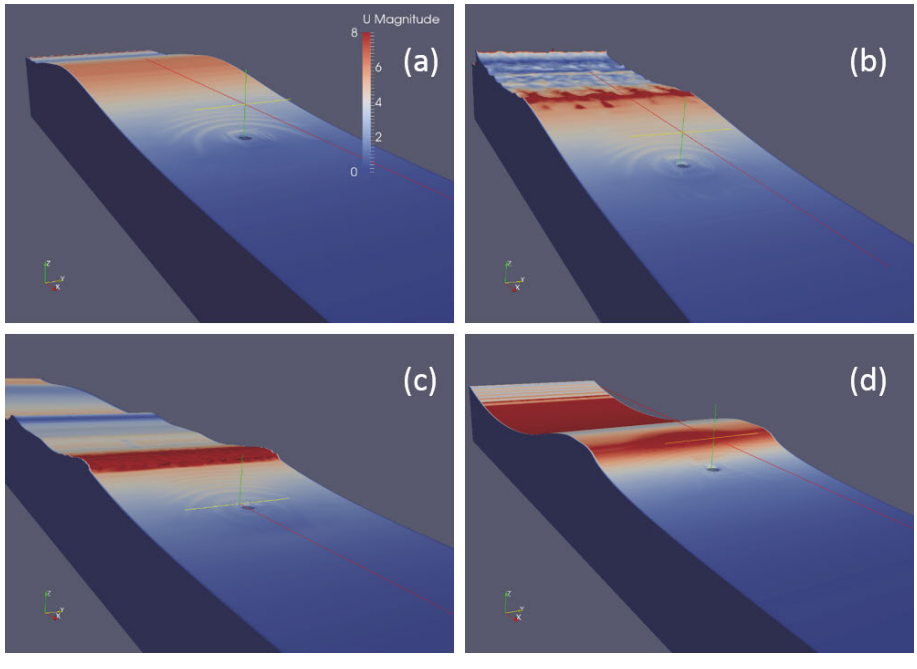

Figure 5.10. Three numerical approaches for tsunami modelling compared with one regular wave. The magnitude of the water velocity at the surface is seen as colour. The waves are propagating from the left to the right. The buoy of a WEC is seen at the moment just before it gets fully submerged.(**a**) The solitary wave. (**b**) The high speed incident current approach. (**c**) The dam-break approach. (**d**) The regular Stokes 5th wave.

In figure 5.10, the wave profiles are seen for the four waves at the moment just before the buoy of the WEC got submerged. The velocity fields and pressure profiles of the modelled waves were compared in paper IV, and it was seen that both the velocity and the pressure were high throughout the whole water column, which is a known characteristics for a tsunami wave. Two of the

approaches, the high speed incident current and the dam-break approach, had a higher water velocity at the surface, and turbulent bores were starting to form. The tsunami waves of those two approaches did also have continuously high water velocity and pressure following the first incident wave peak, whereas the solitary wave was followed by normal pressure and no water velocity. It is concluded that either the high speed incident current approach or the dam-break approach resembles the conditions during a real tsunami event better than the solitary wave. All three modelling approaches resulted in tsunami waves with leading wave peaks, whereas a real tsunami event can begin with a leading wave trough. The surface elevation was initially smooth. As can be seen in figure 5.10, the buoy of the WEC got submerged by the initially smooth surface elevation, and was already submerged when the bore propagated over the WEC. The Stokes 5th wave that was modelled as a regular wave in paper IV was chosen to have the same amplitude as the tsunami waves. It should be noted that since each tsunami wave only had one leading wave peak and no trough, the second wave peak of the Stokes 5th wave was significantly steeper than the tsunami waves, and resulted in higher forces. It should also be noted that although the tsunami waves were realistic, a regular wave of this amplitude is normally not expected at this depth. The modelled Stokes 5th wave could not be considered a deep water wave, since it affected the velocity and the pressure throughout the whole water column.

5.3.2 Forces on the WEC in tsunami waves

When the forces on the WEC by the different tsunami waves and the regular wave were compared in paper IV, it was seen that the peak forces in the connection line were comparable for the modelled tsunami waves, but significantly higher for the Stokes 5th wave. The force on the generator hull was also studied, and the Stokes 5th wave did again result in the highest force. This suggest that if a WEC is designed to survive an extreme wave, it will survive a tsunami wave of the same magnitude. However, it is not obvious that a tsunami wave should be compared with a regular wave of the same amplitude.

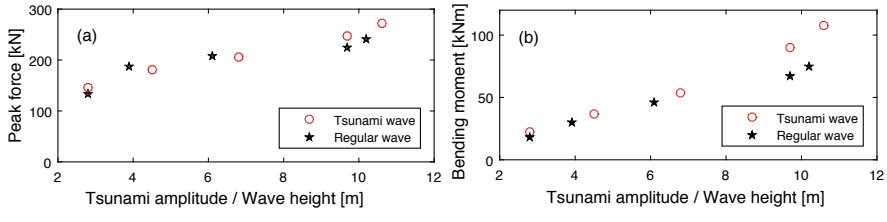

Figure 5.11. The forces on the WEC were comparable when tsunami amplitude was compared with regular wave height. (**a**) Peak forces in the connection line. (**b**) Bending moment on the generator hull at the seabed.

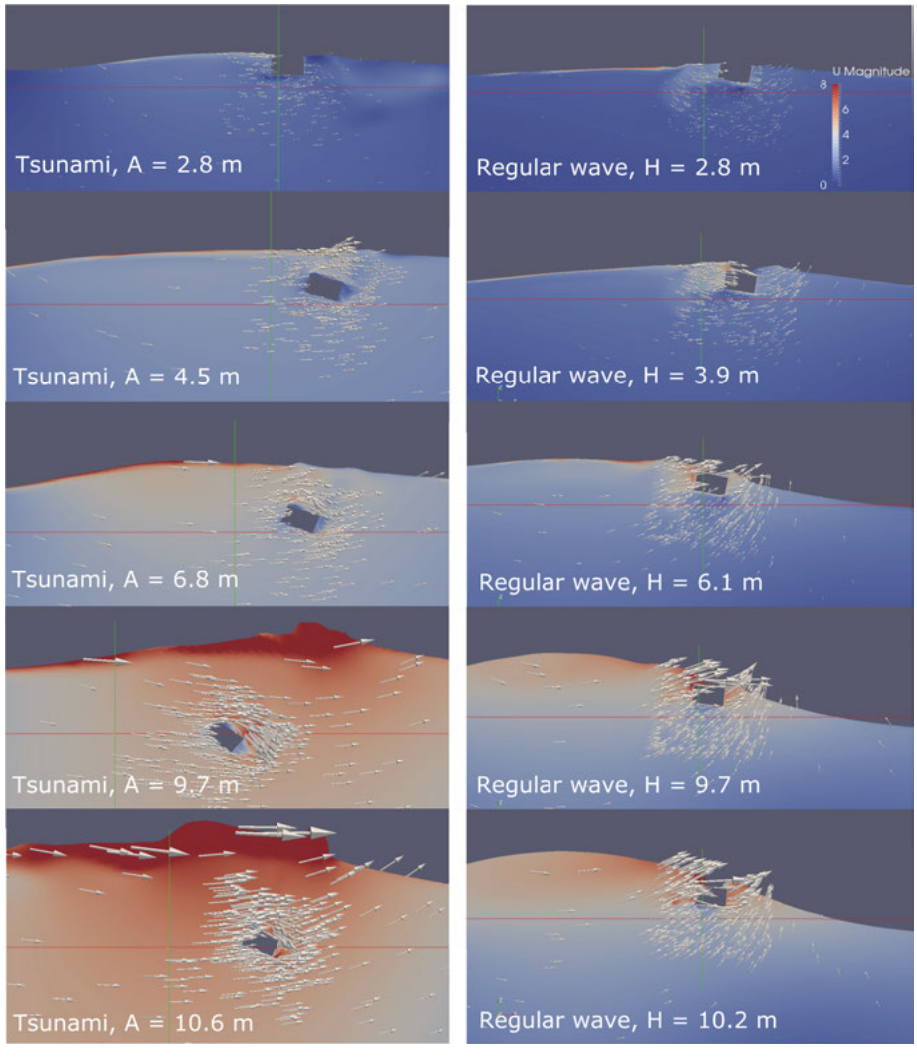

Figure 5.12. The velocity field in the vicinity of the buoy. (Left) Tsunami waves were modelled with the dam-break approach. (Right) Regular waves were modelled as Stokes 5th waves.

In paper V, the dam-break approach was used to model five tsunami events with increasing amplitude, which were compared with five regular waves with wave heights corresponding to the tsunami amplitudes. The line force of the WEC was studied, as well as the bending moment on the generator hull and the heave and surge motion of the buoy. In figure 5.11, the peak force and the bending moment on the generator hull is plotted, comparing the tsunami amplitude with the regular wave height. It is seen that if the WEC parameters are the same and the tsunami wave is propagating with a leading wave peak, the forces on the WEC is comparable when the tsunami amplitude is compared

with regular wave height. In figure 5.12, the velocity field of the tsunami waves and the regular waves are compared in the vicinity of the buoy. It is seen that for the tsunami wave, the buoy was already submerged when the bore of the tsunami wave propagated over the WEC. Although the water at the surface had a much higher velocity for the tsunami wave than for the regular wave, the water with the highest velocity never impacted the buoy due to the limited stroke length of the WEC.

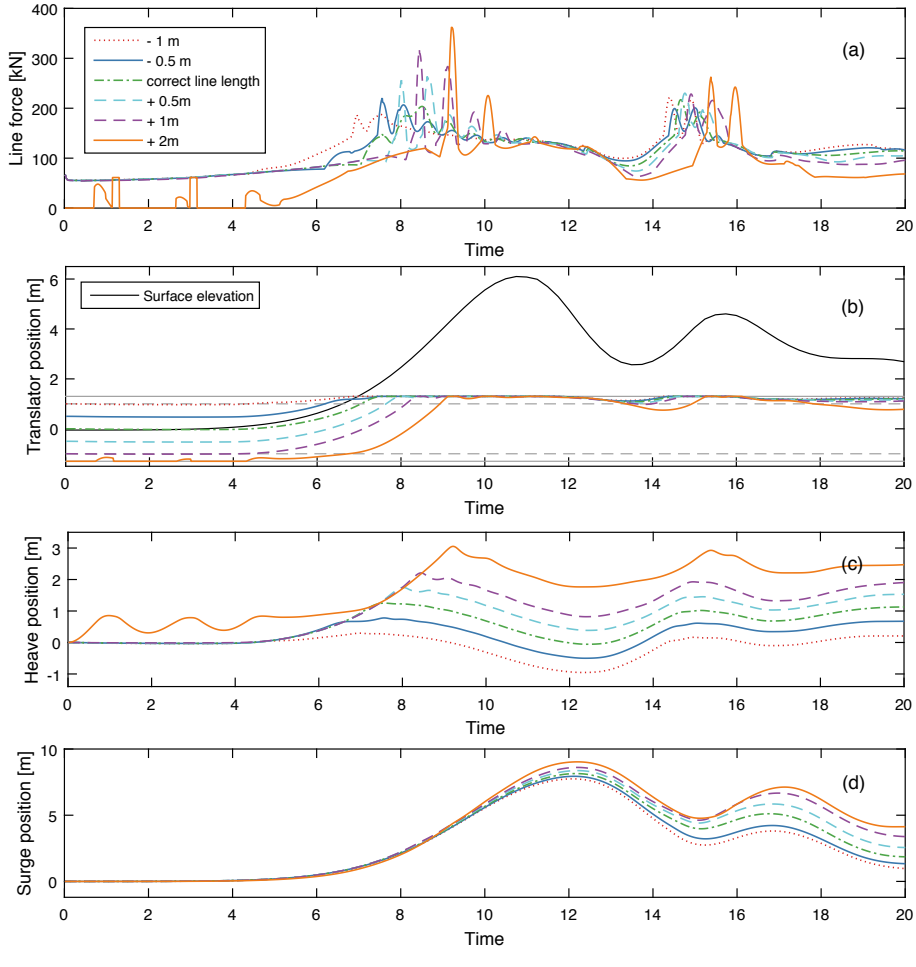

Figure 5.13. The WEC impacted by a tsunami modelled with the dam-break approach, too long connection lines compared with too short lines. (**a**) The force in the connection line. (**b**) Translator position and surface elevation measured right above the WEC. (**c**) The heave motion of the buoy. (**d**) The surge motion of the buoy.

5.3.3 The influence of connection line length

Studying the wave fields in figure 5.12, it can be suggested that the WEC is more vulnerable to a too long connection line if impacted by a tsunami wave than by a regular wave. Since a tsunami event can start with a withdrawal of the water line and a decreased surface level (a leading wave trough), the influence of connection line length is of particular interest to study. In paper VI, a tsunami event was modelled using the the dam-break approach, and the WEC was modelled with both too long and too short line length, while all other parameters were kept constant. In figure 5.13, the line force and the translator position is seen together with the heave and surge motion of the

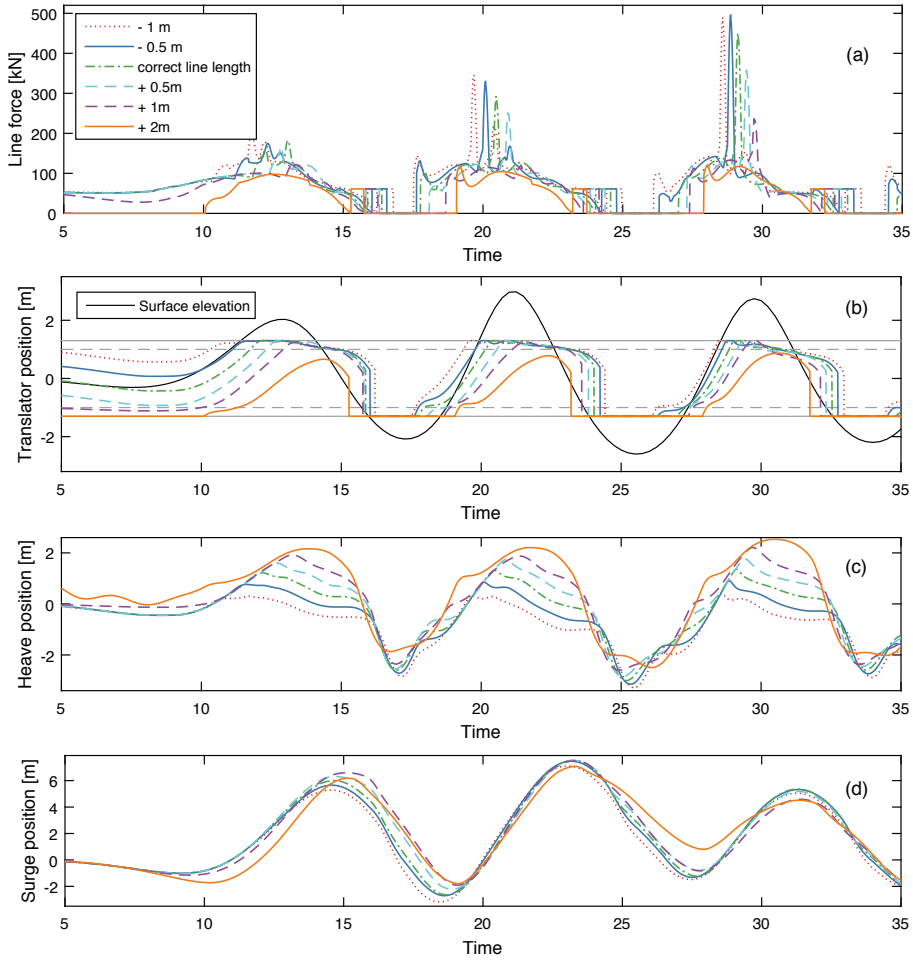

Figure 5.14. The WEC impacted by a regular wave, too long connection lines compared with too short lines. (**a**) The force in the connection line. (**b**) Translator position and surface elevation measured right above the WEC. (**c**) The heave motion of the buoy. (**d**) The surge motion of the buoy.

buoy, comparing the different line lengths when the WEC was impacted by a tsunami wave. It is seen that the peak force in the connection line increased if the line was too long, and decreased if it was too short. Increased line length also increased the buoy motion in both heave and surge. The increased peak line force can be understood as a consequence of the higher water velocity closer to the surface, as was seen in figure 5.12. In figure 5.14, a regular Stokes 5th wave was modelled for comparison. In contrast with the tsunami wave, an increased line length decreased the peak force in the connection line. A too short line increased the peak force, but not to a large extent. It was concluded that a WEC is more vulnerable to line length when impacted by a tsunami wave than by a regular wave. For the regular wave, the too long line increased the heave motion, the same as for the tsunami wave, but the surge motion was decreased. This is a consequence of that the surge motion is influenced by the restricted translator motion; when the translator stand in the upper endstop, the buoy can not move in positive heave direction, and is instead forced to move in surge and/ or in negative heave direction. For the regular wave, the translator never hit the upper endstop for the longest line, and the surge motion was not influenced by the restricted heave motion. For the tsunami wave on the other hand, the translator hit the upper endstop regardless of line length.

5.3.4 The influence of friction on a WEC in a tsunami wave

It was seen in section 5.2.4 that increased friction decreased the peak force of an endstop hit when the WEC was impacted by a regular wave. In this section, the influence of friction is studied when the WEC was impacted by the same tsunami wave that was modelled in section 5.3.3. In figure 5.15, it is seen that increased friction did not decrease the peak force of the endstop hit, but the highest friction results in the highest peak force. The translator position, seen in figure 5.15 (b), suggests that the friction can have contributed to a passive latching by delaying the translator motion and increasing the phase shift between the buoy and the incident wave. For the highest friction, the translator position seems to have been delayed initially, and then increased slightly faster than for lower frictions, which resulted in a higher peak force when the endstop was hit. A similar behaviour is seen in figure 5.16, where the first part of a Stokes 5th wave is shown, when the wave is still increasing in strength from an initially calm sea. Although no friction resulted in the highest peak force, the highest friction did not result in the lowest peak force. It is concluded that for irregular waves, the dynamic WEC behaviour is complex and that conclusions from regular wave experiments should be considered with care.

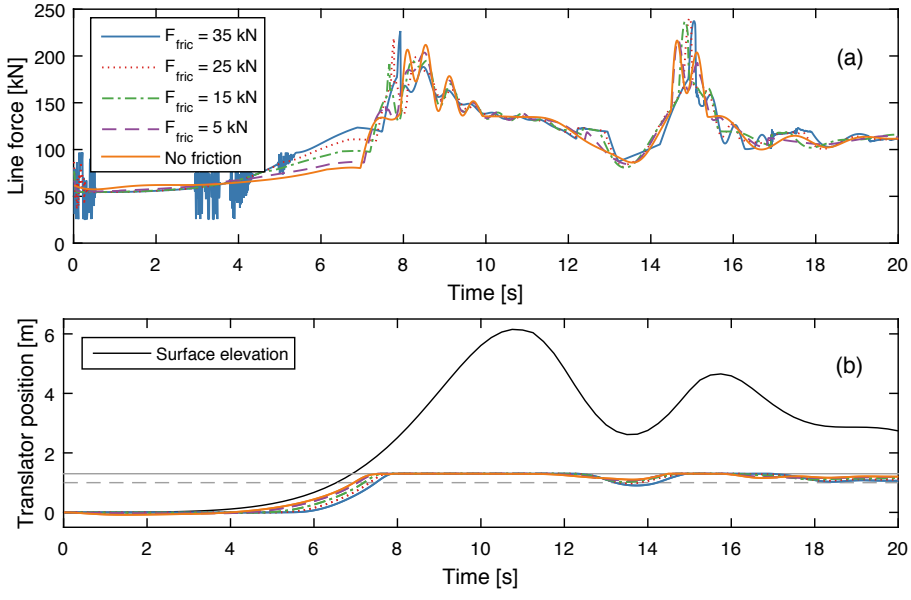

Figure 5.15. The WEC impacted by a tsunami wave, comparing the influence of friction. (**a**) Force in the connection line. (**b**) Translator position and surface elevation measured right above the WEC.

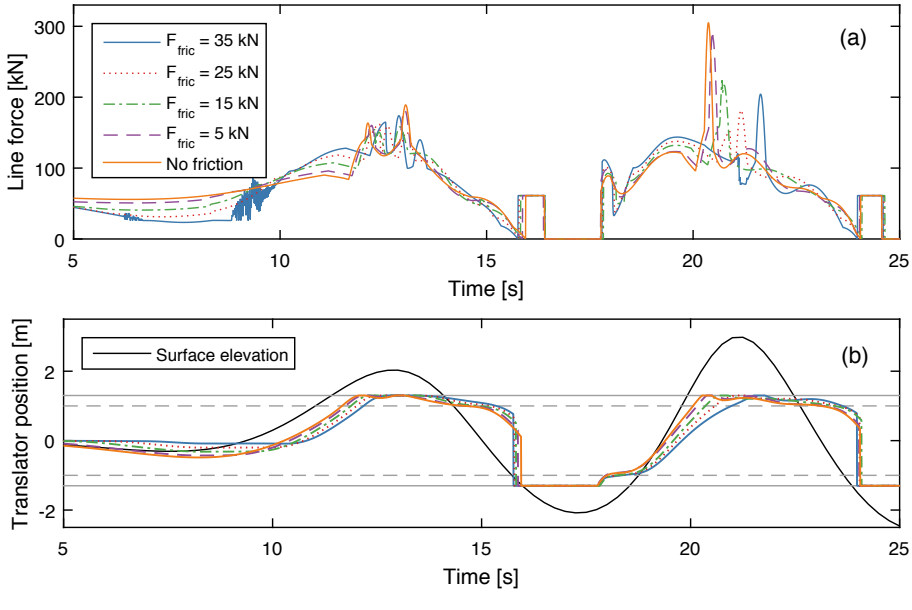

Figure 5.16. The WEC impacted by a regular wave, comparing the influence of friction. (**a**) Force in the connection line. (**b**) Translator position and surface elevation measured right above the WEC.

5.4 WEC behavior with nonlinear PTO system

In paper I-VI, the PTO system has been considered as a linear damper, $F_{PTO} = \gamma\dot{x}$, and/ or a constant frictional force, $F_{fric} = const$. Those are the most commonly studied PTO restraints in the literature, and they are important to study in order to increase our understanding of the dynamic behaviour of the WEC. But as was discussed in section 2.2.2, the assumption of a constant damping coefficient γ is not necessarily a good approximation for all PTO systems. If the linear generator of the Lysekil project is connected to a resistive load, a constant γ is a good approximation only if the inductance of the generator is low, and for low translator speeds. One of the differences between the Nd-Fe-B generator and the ferrite generator is an increased inductance in the ferrite generator, suggesting an increased speed dependence of γ. In paper VIII, the speed dependence of the PTO force was measured onshore, using a crane to lift the translator while the force in the connection line was measured, together with the acceleration, speed and position of the translator. The voltage and current were measured at resistive loads.

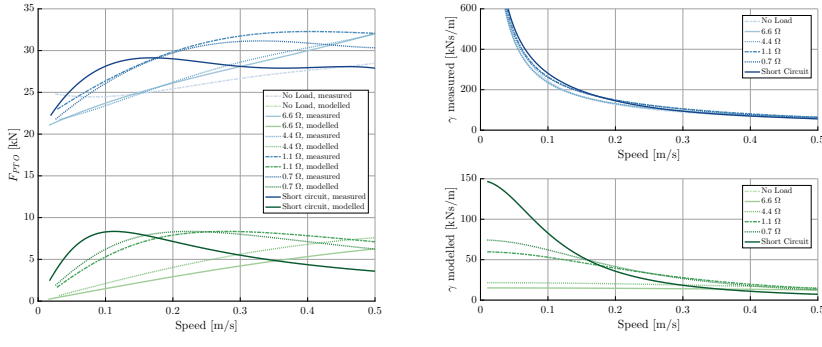

Figure 5.17. (Left) The measured force in the connection line, $F_{PTO}^{mech}(\dot{x})$, (blue) is compared with the force simulated with lumped circuit analysis, $F_{PTO}^{el}(\dot{x})$ (green). Resistive loads were used. (Right) The corresponding damping coefficient γ, as a function of translator speed.

In figure 5.17 (left), the speed dependence of the measured line force is presented with blue lines, for the measured load cases, including no load and short circuit. The blue lines corresponds to the mechanical force in the connection line, $F_{PTO}^{mech}(\dot{x})$, and includes all losses. This can be compared with the green lines, where the measured resistance and inductance were inserted into Eq. (2.5) to model $F_{PTO}^{el}(\dot{x})$. The differences between $F_{PTO}^{mech}(\dot{x})$ and $F_{PTO}^{el}(\dot{x})$ are iron losses and friction. In figure 5.17 (right), the corresponding damping coefficients $\gamma(\dot{x})$ were derived. As can be seen, γ can not be considered independent of the speed if the speed is higher than around 0.05 m/s. A constant γ would be a result of a linearly increasing force in figure 5.17 (left), possibly

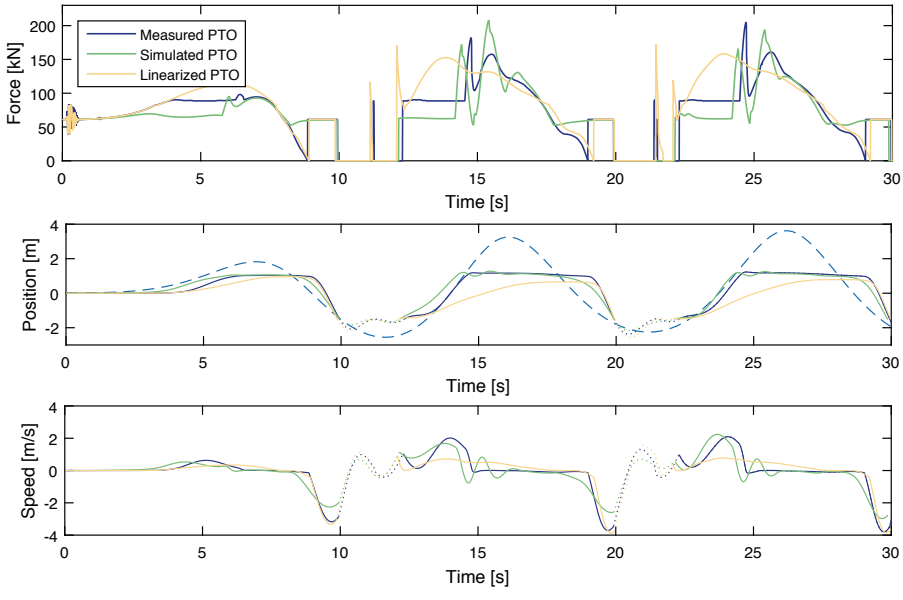

Figure 5.18. WEC behaviour influenced by PTO system, comparing F_{PTO}^{mech}, F_{PTO}^{el} and $F_{PTO}^{linearised}$. The generator was short circuited in the experiment. (**a**) Force in the connection line. (**b**) Translator position and surface elevation measured right above the WEC. The dotted lines marks when the line was slack. The translator position is not known unless the line is tensioned, and the buoy position is instead shown as dotted lines. (**b**) Speed of the translator. The dotted lines show the buoy speed when the line is slack.

with a constant offset: $F_{PTO}^{linearised} = \gamma_{const.}\dot{x} + F_{cons.}$. The discrepancies between F_{PTO}^{mech}, F_{PTO}^{el} and $F_{PTO}^{linearised}$ will have consequences for the produced electricity. However, in this thesis, only the consequences for the damaging peak forces on the WEC in harsh operating conditions have been studied.

In paper VIII, the RANS-VOF model validated in paper I was used to model the WEC behaviour, comparing F_{PTO}^{mech}, F_{PTO}^{el} and $F_{PTO}^{linearised}$ for the three load cases; 1.1 Ω, 6.6 Ω and short circuit. A WEC with a cylinder buoy was modelled as it was impacted by an incident regular wave with a height of 5.9 m and a period time of 10 s. In figure 5.18, the connection line force and the position and speed of the translator is shown for the short circuit case. The experimentally measured PTO system, F_{PTO}^{mech}, corresponds to the solid blue line in figure 5.17 (a), while the modelled PTO system, F_{PTO}^{el}, corresponds to the solid green line. Also, a linear PTO system was modelled for comparison, $F_{PTO}^{linearised} = \gamma_{const.}\dot{x} + F_{cons.}$. In the model, $\gamma_{const.} = 100$ kNs/m and $F_{cons.} = 19.7$ kN, corresponding to the values that would have been measured if the generator was tested at low speed, for example in an overhead crane, and assumed speed independent. It should be noted that the peak forces that

occurred for $F_{PTO}^{linearised}$, yellow lines, and F_{PTO}^{mech}, blue lines, when the connection line had been slack and was stretched again, at t = 12 s and t = 22 s, were consequences of that the translator was not modelled as a separate object. Those peak forces should be disregarded. The resulting differences of WEC behaviour are not neglectable. It is seen that if the WEC was modelled with a linearised PTO system, the damaging peak forces in harsh operating conditions were underestimated. In the second wave peak, at t = 25 s, F_{PTO}^{mech} resulted in lower peak force than F_{PTO}^{el}. For the third wave peak, at t = 25 s, F_{PTO}^{mech} resulted in the highest peak force. In paper VIII, it was concluded that the peak forces will be underestimated if the PTO system is simplified during the design processes. When the different load cases were compared, it was also seen that for this specific generator, the peak forces would be lowest for the 6.6 Ω resistive load case and highest for the short circuit case. This is of particular interest since the highest resistive load results in the lowest damping factor γ if measured at low speed, and if the damping would be assumed linear, this load case would have had the lowest survivability, which is opposite to the result when the nonlinear PTO behaviour was considered.

6. Concluding discussion

For wave energy to be a viable industry, the survivability of the WECs must be analysed and understood. Physical wave tank testing can be performed, but it is expensive and scaled prototypes must be used. Full scale offshore experiments are necessary to prove the concept and to evaluate the WECs offshore performance before commercialisation, but it does not offer the controlled environment and the possibility to repeat the same wave conditions necessary to separate and evaluate the influence of single parameters, not to mention the high cost. Numerical simulations offers a complement to physical experiments where specific parameters can be studied individually at predefined conditions in a numerical wave tank, and to a reasonable cost. Linear potential flow theory has proven accurate during normal operating conditions, and offers a very fast method to calculate the motion of the WECs, and has been used to study linear aspects in paper X-XI. Modelled buoy motion and line force were compared with experimental offshore data in paper X-XI, showing acceptable agreement. But in harsh operating conditions, when the limited stroke length of a WEC is exceeded, the performance of linear models are poor, and fully nonlinear models must be used. RANS-VOF models have proven to have a high accuracy even in turbulent flows, and even though they come with a high computational cost, they have made it possible to study extreme wave events, overtopping, breaking waves, slamming, green water etc. In this thesis, a RANS-VOF model has been developed in the open source software OpenFOAM. It was validated with physical wave tank experiments in paper I, showing good agreement for two different buoy geometries and for different levels of damping.

6.1 WEC survivability

In order to increase the electric power of a WEC, it should be optimized to increase the energy absorption from the waves, and the force in the connection line should be as high as possible. However, to increase the survivability, the force in the connection line should instead be decreased. Those two contradictory design criteria stress the need to study the dynamic behaviour of a WEC, and highlight the benefits of fully nonlinear numerical models, where the peak forces of endstop hits can be studied in time domain and the influence of single parameters can be isolated and compared. In paper I-VI, the validated RANS-VOF model has been used to study how different aspects influence the

survivability of a WEC in extreme waves and tsunami waves. As can be understood from the equation of motion for the translator, an increased generator damping will increase the force in the connection line if the translator speed is constant. However, during offshore operation, the speed of the translator will not be constant, but dependent of the energy in the waves as well as all forces from the generator; PTO damping, friction, gravity and endstop forces. In this thesis, the RANS-VOF model has been used to study the influence of those forces in detail, and it has been seen that increasing the damping forces from the generator decreases the speed of the translator, which decreases the peak forces of endstop hits during offshore operation. Still, the design choices are not trivial. For example, a stiffer endstop spring will increase the peak force that occur when the endstop spring is hit, but if a weaker spring is used, it may become fully compressed and second, higher, peak force will occur. In this thesis, different WEC parameters have been evaluated in the different papers, and the magnitude of the peak forces in the different papers should not be compared unless this is considered.

6.2 Numerical modelling of a WEC in tsunami waves

At deep water, a tsunami wave can be modelled using linear shallow water theory. But when the tsunami wave propagates up on the continental shelf, the wave dynamics is very complex and nonlinear behaviour can not be neglected. In this thesis, the validated and fully nonlinear RANS-VOF model has been used to study the velocity and pressure fields of bore-type tsunami waves with leading wave peaks. The force in the connection line of the WEC and the bending moment on the generator hull at the seabed have been studied. The forces were seen comparable with forces from regular waves, when the tsunami amplitude was compared with regular wave height. It could be concluded that if a WEC is designed to survive a storm induced extreme wave at a site, it would also withstand a tsunami wave of the same magnitude. However, it should be noted that this is not necessarily a fair comparison; at a site with the studied depth of 26 m, the tsunami waves were realistic but the regular wave heights were not typically expected at this depth. Also, for many possible sites in the world, storm induced extreme waves are expected, while tsunami waves are not. Regardless, the comparison showed the benefits of studying tsunami waves with numerical RANS-VOF models; the influence of specific parameters could be separated, and the fully nonlinear velocity and pressure fields could be compared for the different waves. For example, one interesting parameter is the length of the connection line. The peak force in the connection line is influenced by the line length, which was studied in paper VI, where too long and too short line lengths were compared. When the WEC was impacted by a regular wave, an increased line length decreased the peak force. But for the tsunami wave, the increased line length did instead increase

the peak force significantly. This could be explained by studying the buoy motion and translator position and comparing the wave fields. For the regular wave, the increased line length implied that the limited stroke length of the WEC was not reached and the translator never hit the upper endstop. For the tsunami wave on the other hand, the buoy was dragged far away in the surge direction and hit the endstop regardless of line length. When the connection line was too short, the buoy got deeply submerged by an initially smooth surface rise, before the turbulent bore arrived. But when the connection line was too long, the buoy was instead impacted by the bore, which had a significantly higher water velocity. In this thesis, only leading wave peak tsunamis have been studied, while tsunamis can approach with a leading wave trough. From this aspect, the conclusion that a WEC is more vulnerable to a too long line length if impacted by a tsunami wave than by a regular wave is important.

6.3 Nonlinear PTO behaviour

When working with a wave power concept with full scale generator prototypes, it is important to consider the total generator behaviour, including losses and concept specific constrains such as partial translator-stator overlap. In paper VII-IX, the total generator damping was studied experimentally, by measuring the force in the connection line, while a crane was used to lift the translator. Substantial differences were seen between F_{PTO}^{mech}, F_{PTO}^{el} and $F_{PTO}^{linearised}$. The WEC behaviour was modelled with the RANS-VOF model as it was impacted by a high regular wave, comparing the influence of the different PTO restraints. It was seen that the peak forces would be underestimated if the PTO was assumed to behave as a linear damper. In this thesis, only the consequences for the survivability have been considered, but it should be noted that the discrepancies will make substantial differences for the power output of a WEC as well. However, it should also be noted that the damping characteristics for higher speed could be improved by a different loading strategy. Even so, the resistive load case is an important special case for understanding the generator behaviour. Also, at the time this thesis is written, the very same ferrite generator is deployed offshore with resistive load, and the onshore experiments will be necessary to analyse the WECs behaviour offshore.

6.4 Conclusions

The aim of this thesis was to develop a way to study the peak force that occurs when the translator of the linear generator in the the Lysekil project hits the upper endstop, during extreme waves and tsunami waves, and to study how different parameters influence the WEC survivability. This has been achieved by developing a RANS-VOF model in the open source software OpenFOAM.

The model has been validated with physical wave tank data, showing good agreement both for a cylinder buoy and for the more complex buoy geometry cylinder with moonpool. It has then been used to study the survivability of a WEC in both regular extreme waves and tsunami waves. Further, the generator damping of two full scale WECs has been experimentally measured, and the RANS-VOF model has been used to study the consequences of the nonlinear behaviour of the PTO system for a WEC during offshore deployment. It has been concluded that:

- The RANS-VOF model showed good agreement with physical wave tank data and can be used to study the dynamical behaviour of a WEC during normal operating conditions as well as during extreme wave events and tsunami waves.
- For regular waves, it was seen that both increased linear generator damping, $F_{PTO} = \gamma \dot{r}$, or increased constant damping, $F_{fric} = constant$, decreased the peak force of the endstop hits. This corresponds well with established experimental results.
- For non-periodic waves; during a tsunami event or the transient at the front of a regular wave train, it was seen that increased friction could result in a latching effect and actually increase the force of the endstop hit instead of decreasing it. It is possible that this effect also could occur for irregular waves during normal operating conditions.
- When the tsunami waves with leading wave peaks of certain amplitude were compared with regular waves with corresponding wave height, it was seen that the peak force in the connection line was comparable when the line length was correct, and for realistic WEC parameters. In this comparison, the bending moment on the generator hull was 42 % higher for the highest tsunami wave than for the corresponding regular wave.
- Due to the differences in fluid velocity fields, the WEC was more vulnerable to a too long line length when impacted by a tsunami wave than by a regular wave. For a regular wave, an increased line length resulted in lower endstop forces and decreased surge motion. For the tsunami wave on the other hand, an increased line length resulted in significantly higher endstop forces.
- The experimentally measured PTO damping of the full scale ferrite generator was nonlinear. The RANS-VOF model was used to study the consequences for survivability of the experimentally measured PTO behaviour, and it was seen that if the generator behaviour was assumed linear, the peak forces in the connection line would be underestimated.

7. Summary of Papers

This chapter provides a summary of the papers included in this thesis. The fully nonlinear RANS-VOF model was presented and verified in paper I. In paper II-VI, the RANS-VOF model was used to study parameters influencing the survivability of the WEC in extreme waves, such as buoy geometry, overtopping, linear PTO damping, friction and connection line length. The response in regular extreme waves is compared with tsunami wave events in paper IV-VI. Since a WEC's behaviour is highly dependent on the PTO system, paper VII was experimental and measured the mechanical PTO force in the connection line, including mechanical and electrical losses. The experiment was performed on a full scale Nd-Fe-B generator at constant speed. A ferrite generator is expected to have an increased speed dependent behaviour, and in paper VIII-IX the nonlinear PTO behaviour including all losses was measured. The RANS-VOF model was then used to study the influence of the discrepancies between the measured behaviour and an assumed linear PTO system. Paper X and paper XI, where linear potential flow theory was used to study power absorption of a WEC during normal operating conditions, are also included in this thesis.

Paper I

Numerical Models for the Motion and Forces of Point-absorbing Wave Energy Converters in Extreme Waves

This paper presents three numerical models; one linear Matlab model and two fully nonlinear RANS-VOF models built in OpenFOAM and ANSYS Fluent, respectively. The force in the connection line of a WEC was studied, as well as the heave and surge motion of the buoy, in high waves and during an extreme wave event. The models were compared with each other and with physical wave tank data. Both nonlinear models showed good agreement with the physical wave tank data, while the linear model was not considered accurate enough to study the force of the endstop hits.

The author developed the OpenFOAM model and analysed and compared the data presented in the paper. The author also wrote a major part of the paper.

The paper is published in Ocean Engineering, September 2017.

Paper II

Buoy Geometry and its Influence on Survivability for a Point-absorbing Wave Energy Converter: Scale Experiment and CFD Simulations

The influence of buoy geometry on the force in the connection line of a WEC was studied, using both physical wave tank data and the OpenFOAM RANS-VOF model. A cylinder buoy was compared with a buoy with a moonpool. The buoy with the moonpool was seen to yield slightly lower peak forces, but it should be noted that it is also expected to have a lower power absorption due to its lower added mass.

The author performed the numerical modelling and wrote a major part of the paper.

The paper is a peer reviewed extended abstract presented at the Marine Energy Technical Symposium, Washington DC, United States of America, May 1-3 2017.

Paper III

The Effect of Overtopping Waves on Peak Forces on a Point-absorbing WEC

In this paper, the OpenFOAM RANS-VOF model was used to study the influence of overtopping waves on the peak forces. It was seen that if the limited stroke length of the WEC was exceeded and the endstop spring was hit, overtopping did not influence the magnitude of the peak forces. If the PTO damping was high enough to prevent an endstop hit, the peak forces were seen to level out even for the higher waves in the paper.

The author did the majority of the work.

The paper is published in the proceedings of the 3rd Asian Wave and Tidal Energy Conference Series, Singapore, Singapore, October 24-28 2016.

Paper IV

Peak Forces on a Point-Absorbing Wave Energy Converter Impacted by Tsunami Waves

This paper compared three numerical approaches for modelling of tsunami waves at intermediate depth; a solitary wave, a dam break-break approach and a high speed incident current. The velocity and pressure fields were compared, and the impact of the waves on a WEC was studied. A high regular wave of comparable wave height was modelled for comparison, and it was seen that both the force in the connection line and the force on the generator hull was higher when the WEC was impacted by the regular wave than by the tsunami.

The author did the majority of the work.

The paper is under review for Renewable Energy, 2017.

Paper V

Survivability of a Point-Absorbing Wave Energy Converter Impacted by Tsunami Waves

One of the numerical approaches that was studied in paper IV, the dam-break approach, was chosen to model tsunami waves of increasing amplitude and study the impact on a WEC. Regular waves were modelled for comparison, and it was seen that when the tsunami wave of a certain amplitude was compared with a regular wave of the same wave height, both the force in the connection line and the bending moment on the generator hull were comparable. When the dam-break approach is utilized with wet bed condition, the tsunami wave will approach with a leading wave peak, and it was noted that the buoy was submerged before the highest wave peak arrived, and thereby not impacted by the highest water velocity in the turbulent bore.

The author did the majority of the work.

The paper is published in the proceedings of the 12th European Wave and Tidal Energy Conference Series, Cork, Ireland, August 24-28 2017.

Paper VI

Peak Forces on Wave Energy Linear Generators in Tsunami and Extreme Waves

In this paper, the RANS-VOF model was used to study the influence of linear PTO damping and friction. It was seen that for periodic waves, both linear PTO damping and friction, assumed constant, decreased the forces of the endstop hits. For irregular waves however, the transient front of the wave train and in a tsunami wave, an increased friction did not always result in a decreased peak force, but a latching effect could occur, increasing the peak force instead of decreasing it. The dam-break approach was used to model a tsunami wave with a leading wave peak. Since a tsunami wave event can approach with a leading wave trough and decreased water level, the effect of too long or too short connection line was studied and the results compared with a regular wave. It was seen that while an increased line length gave a protective effect when the WEC was impacted by a high regular wave, the peak forces increased significantly when the connection line was too long during the tsunami event. This was explained by the differences in the wave fields. If the length of the connection line was correct or too short, the buoy got submerged by the initial smooth surface rise of the tsunami event, and the turbulent bore propagated over the deeply submerged buoy. But if the line was too long, the buoy was instead impacted by the turbulent bore, and the peak force increased.

The author did the majority of the work.

The paper is published Energies, September 2017.

Paper VII

Line Force and Damping at Full and Partial Stator Overlap in a Linear Generator for Wave Power

In an onshore experiment, the force in the connection line of a full scale Nd-Fe-B generator was measured throughout the full translator stroke length. The measured line force, generator damping and stator overlap were studied in relation to translator speed by comparing the line force and the damping coefficient, γ, for multiple load cases along the translator stroke length. Two constant translator speeds were used in this paper.

The author contributed to the experimental design and to the writing of the paper.

The paper is published in Journal of Marine Science and Engineering, November 2016.

Paper VIII

Speed Dependent PTO Damping in a Linear Generator for Wave Power - Measured Damping and Simulated WEC Behaviour

Since a ferrite generator is expected to have an increased induction and consequently increased speed dependence of the generator damping coefficient γ, this paper measured the speed dependence of the force in the connection line and of γ. This was measured in two ways; first using a force sensor in the connection line to find the mechanical force that the buoy would experience during operation, F_{PTO}^{mech}, including all losses. Secondly, the measuring current and voltage was used to derive the electrical force, F_{PTO}^{el}, where only the copper loss was included. F_{PTO}^{mech} is the force that the buoy would experience during operation, while F_{PTO}^{el} is the force that would be derived if only the voltage and current were measured during operation. The OpenFOAM RANS-VOF model was used to study how the discrepancies between F_{PTO}^{mech} and F_{PTO}^{el} affected the force of the endstop hits when a WEC was impacted by a high regular way. The behaviour of an assumed linear PTO system was also modelled for comparison. This paper was limited to study the generator during full translator-stator overlap.

The author contributed to the design and the execution of the experiment. The author performed the RANS-VOF modelling and wrote parts of the paper.

The paper is under review for Journal of Marine Science and Engineering, August 2017.

Paper IX

Experimental Study of Generator Damping at Partial Stator Overlap in a Linear Generator for Wave Power

The generator behaviour during partial translator-stator overlap was studied experimentally in this paper. The force from the generator was described as $F_{PTO}A_{frac}^{c}$, where A_{frac} was the fraction of the stator overlapped by translator. The factor c was experimentally studied in this paper.

The author's contribution was mainly experimental.

The paper is published in the proceedings of the 12th European Wave and Tidal Energy Conference Series, Cork, Ireland, August 24-28 2017.

Paper X

On the Optimization of Point-Absorber Buoys

The buoy motion response to irregular waves was modelled using a linear model and the influence of buoy draft and radius on power absorption was studied. The power absorption was compared with results from offshore experiments including two full scale WECs. The sea state was chosen with a significant wave height of $H_s = 1.05$ m, the free stroke length was never exceeded and the endstop spring never impacted. Acceptable agreement was found, and it was concluded that linear potential flow theory is an acceptable approximation during normal operating conditions and when the endstop spring is not hit.

The author performed the simulations, analysed the results and wrote the paper.

The paper is published in Journal of Marine Science and Engineering, May 2014.

Paper XI

Calculating Buoy Response for a Wave Energy Converter - a Comparsion Between Two Computational Methods and Experimental Results

In this paper, a linear model was built in COMSOL Multiphysics to solve for the hydrodynamic parameters of a point-absorbing WEC. The results were compared with a linear model where the hydrodynamical parameters were computed using WAMIT, and to experimental results from the Lysekil research site. The agreement with experimental data was good for both numerical models.

The author performed the simulations, analysed the results and wrote the paper.

The paper is published in Theoretical and Applied Mechanics Letters, 2017.

8. Svensk sammanfattning

Havets vågor transporterar enorma mängder energi. Energin i vågorna på havsytan är ursprungligen solenergi som värmer atmosfären och skapar vindar. Friktion mellan vindarna och havets vattenyta skapar vågor. Vågorna kan transportera energi över mycket stora områden med små energiförluster, innan de når grundare vatten och energin övergår till värme genom friktionsförluster mot botten och i brytande vågor. Vågenergi är både förnybar, energität och mer förutsägbar än vindkraft, och om den kunde omvandlas till exempelvis electricitet så skulle den kunna erbjuda ett bra bidrag till världens energiefterfrågan. Vi människor har alltid fascinerats över vågornas kraft, och det allra första vågkraftspatentet beviljades redan år 1799. Det var dock först i samband med oljekrisen på 1970-talet som forskningen om vågkraft tog fart på allvar. Idag har mer än 1000 koncept föreslagits och åtskilliga av dem har tagit sig från ritbordet till småskaliga prototyper. Ett fåtal har kommit så långt som till fullskaliga prototyper i drift. Men att få en prototyp att överleva till havs och fortfarande vara ekonomiskt gångbar är inte trivialt, och än så länge råder det ingen konsensus om vilket koncept som kommer kunna visa sig ekonomiskt hållbart. I dagsläget måste vågkraft betraktas som ett forskningsområde snarare än en mogen industri. Man kan fråga sig vad det är som är så svårt? Offshore-industri går ju bra, och vi har ju byggt båtar i tusentals år? Men även om vågkraftsforskningen har kunnat dra nytta av de tekniska framstegen inom den traditionella offshore-industrin, så får vi inte glömma att det finns viktiga skillnader. Till exemple så designas ett skepp eller en offshore-plattform för att påverkas så lite som möjligt av vågorna, och strukturens resonansfrekvenser får inte sammanfalla med havsvågornas frekvenser. Ett vågkraftverk designas däremot för att maximera den energi som absorberas från vågorna, bland annat genom resonans.

Forskningen inom vågkraft har till en början fokuserat framför allt på att optimera koncepten för maximal energiabsorbtion, till vilket linjära modeller fungerar bra. Men för att studera driftsäkerhet och överlevnad under svåra driftförhållanden så måste även icke-linjära aspekter studeras, till exempel turbulens och översköljande vågor. Fokuset i denna avhandlingen är att studera beteende och krafter på ett vågkraftverk i stormar och vid tsunamivågor. Det vågkraftskonsept som har studerats är en så kallad "point-absorber", där en linjär generator på botten drivs direkt av en boj på ytan. Bojen är koppad till en translator inne i generatorn via en stållina. Bojen är liten i förhållande till våglängden, vilket innebär att den vid dess resonansfrekvens kan absorbera

energi från ett stort område, större än dess diameter. Den linjär generatorn har en begränsad slaglängd, vilket gör att translatorn som rör sig inne i generatorn kommer slå i toppen på generatorn om vågorna är för höga, med höga maxkrafter som följd. En icke-linjär beräkningsmodell har utvecklats i mjukvaran OpenFOAM. Modellen har verifierats med hjälp av vågtankstester, med mycket gott resultat. OpenFOAM-modellen har sedan använts för att studera hur olika aspekter och parameterar påverkar vågkraftverket, både vid höga reguljära vågor och vid tsunamis. Övertoppande vågor har studerats, samt hur kraft och rörelse påverkas av bojgeometri. Både konstant och linjär generatordämpning har studerats, och hur maxkrafterna på vågkraftverket påverkas av för kort eller för lång stållina.

För periodiska vågor har det visats att både en ökad konstant dämpning eller en ökad linjär dämpning minskar de skadliga maxkrafterna när generatorns slaglängd överskrids. Men för icke-periodiska vågor, dels tsunamivågor samt den inledande transienten i början av ett vågtåg, så var detta samband inte alltid giltigt. En konstant dämpning, till exempel friktion, kunde under vissa förhållanden öka islagskraften istället för att minska den. Detta berodde på att en hög friktion initialt kunde hålla nere translatorn medan bojen drogs in i vågen. När vågen sedan lyfte bojen så fick translatorn en högre fart, vilket ökade kraften när translatorn slog i toppen.

En tsunamivåg på djupt vatten är relativt enkel att modellera numeriskt, men när den propagerar upp på kontinentalplattan så förändras dess beteende och icke-linjära effekter blir långt ifrån försumbara. På djupt vatten kan en tsunami beskrivas med linjär teori, och på mycket grunt vatten och på land så används ofta både småskaliga fysiska och fullskaliga numeriska dammbrottsmodelleringar. Men i dagsläget råder det inte konsensus om hur tsunamivågor på relativt grunt vatten, där vågkraftverk vanligtvis sjösätts, bör modelleras. I denna avhandling har därför tre numeriska metoder för modellering av tsunamivågor på 26 m djupt vatten jämförts: en solitär våg, ett dammbrott uppe på en vattenvolym med ett djup på 26 m, samt en metod där strömmande vatten med hög hastighet tvingades in i en initiallt stilla vattenvolym. Alla tre metoderna resulterade i tsunamivågor med ledande vågtopp. Eftersom en tsunami kan ha en ledande vågdal, vilket resulterar i att vattennivån först sjunker och att kustlinjen drar sig tillbaka, så användes OpenFOAM-modellen till att studera hur ett vågkraftverks linlängd påverkade vågkraftverket när det träffades av en tsunamivåg. Modelleringen visade att en för lång lina hade en skyddande effekt om vågkraftverket påverkades av höga, reguljära vågor, men om det istället träffades av en tsunamivåg så ökade tvärt emot den skadliga islagskraften om linan var för lång.

9. Acknowledgement

First of all, I would like to thank my main supervisor Malin Göteman, for your endless guidance and support. You are one of the most intelligent, professional, inspiring, yet very nice person I have ever met, and a true role model for me. I would also like to thank my first main supervisor, Magnus Rahm, for guiding me through my early years as a young PhD student, thank you! I would like to express my gratitude to Mats Leijon, for giving me the opportunity to perform my PhD studies at the Division of Electricity, and to Center for Natural Disaster Science (CNDS), for supporting my research. And thanks to UPPMAX for making 20000 (cpu)hours weeks possible. The computations were performed on resources provided by the Swedish National Infrastructure for Computing (SNIC) at UPPMAX.

Thanks to all my colleagues and friends that I have met at the Division of Electricity! Thanks for every trip to Lysekil; regardless of resulting progress, it has always been nice to share the work with friends. Thanks to Maria Angeliki for always bringing sweets. Thanks to Ling and Yue, for your hard work. Thanks to Rafael and Tobias, for every Lysekil trip. Thanks to Liselotte for all our totally perfect heavy lifting and for harpooning. Thanks to Anders for welding the great harpoons. And thanks to all persons at Seabased who has helped us out, Daniel, Nelly, Tommy, Kathe, Boel and everyone else! Thanks to Victor for helping me out with OpenFOAM. Thanks to everyone who has shared an office with me: Mårten, Katarina, Anders, Johan, Valeria, Birger, Liselotte, Nicole, Fredrik and Stefan. And thanks for every evening in the bar! Thanks to Mikael for keeping up this tradition, so important for our joint research efforts. And thanks to everyone at the sushi-list, and thanks to Morgan, Liselotte and Anna for keeping up also this tradition, equally important for our research efforts. And thanks to everyone else here at the Division of Electricity! For making my years here a good time.

Thank you mom, for raising me the person I am. And thank you dad, for your unquestionable faith in me. And thank you Emil, for being my brother, always there when I need you.

I would also like to thank my husband Stefan. Words can not express what you means to me. I love you. And thanks to our amazing daughter Anna, you are the best!

And finally, an acknowledgement to every lost buoy out there: hang in there.

References

[1] A. Clement, P. McCullen, A. Falcao, A. Fiorentino, F. Gardner, K. Hammarlund, G. Lemonis, T. Lewis, K. Nielsen, S. Petroncini, M. T. Pontes, P. Schild, B. Sjöstrom, H. C. Sørensen, and T. Thorpe, "Wave energy in europe: current status and perspectives," *Renewable and Sustainable Energy Reviews*, vol. 6, pp. 405–431, 2002.

[2] I. Lopez, J. Andreu, S. Ceballos, I. Alagria, and I. Kortabarria, "Review of wave energy technologies and the necessary power-equipment," *Renewable and Sustainable Energy Reviews*, vol. 27, pp. 413–434, 2013.

[3] A. Falcao, "Wave energy utilization: a review of the technologies," *Renewable and Sustainable Energy Reviews*, vol. 14, pp. 899–918, 2010.

[4] S. Astariz and G. Iglesias, "The economics of wave energy: A review," *Renewable and Sustainable Energy Reviews*, vol. 45, pp. 397–408, 2015.

[5] S. Astariz and G. Iglesias, "Wave energy vs. other energy sources: A reassessment of the economics," *International Journal of Green Energy*, vol. 13, pp. 747–755, 2016.

[6] A. Day, A. Babarit, A. Fontaine, Y. He, M. Kraskowski, M. Murai, I. Penesis, F. Salvatore, and H. Shin, "Hydrodynamic modeling of marine renewable energy devices: A state of the art review," *Ocean Engineering*, vol. 108, pp. 46–69, 2015.

[7] J. Falnes, *Ocean waves and oscillating systems*. The press syndicate of the University of Cambridge, United Kingdom, 2004.

[8] http://www.pico-owc.net/, access date 31 May 2017.

[9] Y. Masuda and M. McCormick, "Experiences in pneumatic wave energy conversion in japan," *McCormick ME, Kim YC, editors. Utilization of ocean waves - wave to energy conversion. New York ASCE*, pp. 1–33, 1987.

[10] http://www.wavedragon.net/, access date 31 May 2017.

[11] B. Drew, A. Plummer, and M. Sahinkaya, "A review of wave energy converter technology," *Proceedings of the Institution of Mechanical Engineers, Part A: Journal of Power and Energy*, vol. 223, pp. 887–782, 2016.

[12] http://www.emec.org.uk/about-us/wave-clients/pelamis-wave-power, access date 31 May 2017.

[13] J. Chaplin, F. Farley, M. Prentice, R. Rainey, S. Rimmer, and A.Roach, "Development of the anaconda all-rubber wec," *Proceedings of the 7th European Wave and Tidal Energy Conference, Porto, Portugal*, 2007.

[14] http://www.emec.org.uk/about-us/wave-clients/corpower-ocean/, access date 31 May 2017.

[15] http://carnegiewave.com, access date 31 May 2017.

[16] K. Budal and J. Falnes, "A resonant point absorber of ocean-wave power," *Nature*, vol. 256, pp. 478–479, 1975.

[17] S. Salter, "Wave power," *Nature*, vol. 249, pp. 720–724, 1974.

[18] M. Leijon, R. Waters, M. Rahm, O. Svensson, C. Bodström, E. Strömstedt, J. Engström, S. Tyrberg, A. Savin, H. Gravråkmo, H. Bernhoff, J. Sundberg, J. Isberg, O. Ågren, O. Danielsson, M. Eriksson, E. Lejerskog, B. Bolund, S. Gustafsson, and K. Thorburn, "Catch the wave to electricity," *IEEE Power and Energy Magazine*, 2009.

[19] M. Leijon, C. Bodström, O. Danielsson, S. Gustafsson, K. Haikonen, O. Langhamer, E. Strömstedt, M. Stalberg, J. Sundberg, O. Svensson, S. Tyrberg, and R. Waters, "Wave energy from the north sea: Experiences from the lysekil research site," *Surv Geophysics*, vol. 29, pp. 221–240, 2008.

[20] O. Svensson, *Experimental Results from the Lysekil Wave Power Research Site*. PhD thesis, Uppsala University, 2012.

[21] E. Strömstedt, *Submerged Transmission in Wave Energy Converters - Full Scale In-Situ Experimental Measurements*. PhD thesis, Uppsala University, 2012.

[22] M. Stalberg, R. Waters, O. Danielsson, and M. Leijon, "Influence of generator damping on peak power for a direct drive wave energy converter," *Journal of Offshore Mechanics and Arctic Engineering*, vol. 130, 2008.

[23] R. Waters, M. Stalberg, O. Danielsson, O. Svensson, S. Gustafsson, E. Strömstedt, M. Eriksson, and M. Leijon, "Experimental results from sea trials of an offshore wave energy system," *Applied Physics Letters*, vol. 90, 2007.

[24] R. Waters, M. Rahm, M. Eriksson, O. Svensson, E. Strömstedt, C. Boström, J. Sundberg, and M. Leijon, "Ocean wave energy absorption in response to wave period and amplitude offshore experiments on a wave energy converter," *IET Renewable Power Generaton*, vol. 5, pp. 465–469, 2011.

[25] R. Waters, *Energy from Ocean Waves*. PhD thesis, Uppsala University, 2008.

[26] M. Rahm, O. Svensson, C. Boström, R. Waters, and M. Leijon, "Experimental results from the operation of aggregated wave energy converters," *IET Renewable Power Generation*, vol. 6, pp. 149–160, 2012.

[27] M. Rahm, C. Boström, O. Svensson, M. Grabbe, F. Bulow, and M. Leijon, "Laboratory experimental verification of a marine substation," *Proceedings of the 8th European Wave and Tidal Energy Conference, Uppsala, Sweden*, 2009.

[28] M. Rahm, C. Boström, O. Svensson, M. Grabbe, F. Bulow, and M. Leijon, "Offshore underwater substation for wave energy converter arrays," *IET Renewable Power Generation*, vol. 4, pp. 602–612, 2010.

[29] M. Rahm, *Ocean Wave Energy - Underwater Substation System for Wave Energy Converters*. PhD thesis, Uppsala University, 2010.

[30] E. Lejerskog, *Theoretical and Experimental Analysis of Operational Wave Energy Converters*. PhD thesis, Uppsala University, 2016.

[31] C. Boström, *Electrical Systems for Wave Energy Conversion*. PhD thesis, Uppsala University, 2011.

[32] S. Apelfröjd, *Grid Connection of Permanent Magnet Generator Based Renewable Energy Systems*. PhD thesis, Uppsala University, 2016.

[33] R. Krishna, *Grid Connected Three-Level Converters - Studies for Wave Energy Conversion*. PhD thesis, Uppsala Universitet, 2014.

[34] R. Ekström, *Offshore Marine Substation for Grid-Connection of Wave Power Farms*. PhD thesis, Uppsala University, 2014.

[35] B. Ekergård, *Full scale Applications of Permanent Magnet Electromagnetic Energy Converters - from $Nd_2Fe_{14}B$ to Ferrite*. PhD thesis, Uppsala University, 2013.
[36] M. Eriksson, J. Isberg, and M. Leijon, "Therory and experiment on a elastically moored cylindrical buoy," *IEEE Journal of Oceanic Engineering*, vol. 31, pp. 959–963, 2006.
[37] M. Eriksson, *Modelling and Experimental Verification of Direct Drive Wave Energy Conversion*. PhD thesis, Uppsala University, 2007.
[38] L. Hai, *Modelling Wave Power by Equivalent Circuit Theory*. PhD thesis, Uppsala University, 2015.
[39] Y. Hong, *Numerical Modelling and Mechanical Studies on a Point Absorber Type Wave Energy Converter*. PhD thesis, Uppsala University, 2016.
[40] L. Wang, *Modelling and Advanced Control of Fully Coupled Wave Energy Converters Subject to Constraints: the Wave-to-wire Approach*. PhD thesis, Uppsala University, 2017.
[41] W. Li, *Numerical Modelling and Statistical Analyses of Ocean Wave Energy Converters and Wave Climate*. PhD thesis, Uppsala University, 2016.
[42] V. Castellucci, *Sea Level Compensation System for Wave Energy Conversion*. PhD thesis, Uppsala University, 2016.
[43] A. Savin, O. Svensson, E. Strömstedt, C. Boström, and M. Leijon, "Determining the service life of a steel wire under a working load in the wave energy converter," *Proceedings of the ASME 28th International Conference on Ocean, Offshore and Arctic Engineering, OMAE2009 Honolulu, Hawaii*, 2009.
[44] O. Svensson and M. Leijon, "Peak force measurements on a cylindrical buoy with limited elastic mooring," *IEEE Journal of Oceanic Engineering*, vol. 39(2), pp. 398–403, 2014.
[45] A. Savin, *Experimental Mesurement of Lateral Force in a Submerged Single Heaving Buoy Wave Energy Converter*. PhD thesis, Uppsala University, 2012.
[46] A. Savin, O. Svensson, and M. Leijon, "Azimuth-inclination angles and snatch load on a tight mooring system," *Ocean Engineering*, 2011.
[47] A. Savin, O. Svensson, and M. Leijon, "Estimation of stress in the inner framework structure of a single heaving buoy wave energy converter," *IEEE Journal of Oceanic Engineering*, vol. 37, 2012.
[48] H. Gravråkmo, *Buoy Geometry, Size and Hydrodynamics for Point Absorber Linear Wave Energy Converter*. PhD thesis, Uppsala University, 2014.
[49] M. Göteman, J. Engström, M. Eriksson, M. Leijon, M. Hann, E. Ransley, and D. Greaves, "Wave loads on a point-absorbing wave energy device in extreme waves," *Journal of Ocean and Wind Energy*, vol. 2(3), pp. 176–181, 2015.
[50] R. Ekström, B. Ekergård, and M. Leijon, "Electrical damping of linear generators for wave energy converters - a review," *Renewable and Sustainable Energy Reviews*, vol. 42, pp. 116–128, 2015.
[51] M. Eriksson, R. Waters, O. Svensson, J. Isberg, and M. Leijon, "Wave power absorption: Experiments in open sea and simulation," *Journal of Applied Physics*, vol. 102, 2007.
[52] C. Boström, O. Svensson, M. Rahm, E. Lejerskog, A. Savin, E. Strömstedt, J. Engström, H. Gravråkmo, K. Haikonen, R. Waters, D. Björkl"of, T. Johansson, J. Sundberg, and M. Leijon, "Design proposal of electric system

for linear generator wave power plants," *Proceedings of the IEEE Industrial Electronics IECON2009, Porto Portugal*, 2009.
[53] C. Boström and M. Leijon, "Operation analysis of a wave energy converter under different load conditions," *IET Renewable Power Generation*, vol. 5, pp. 245–250, 2010.
[54] R. T. Hudspeth, *Waves and Wave Forces on Costal and Ocean Structures*. World Scientific Publishing Co. Pte. Ltd., 2006.
[55] C. Mei, M. Stiassnie, and D. Yue, *Theory and Applications of Ocean Surface Waves, part 1: Linear Aspects*. World Scientific Publishing Co. Pte. Ltd., 2005.
[56] S. A. Mavrakos and P. McIver, "Comparison of methods for computing hydrodynamic characteristics of arrays of wave power devices," *Applied Ocean Research*, vol. 19, pp. 283–291, 1997.
[57] J. Falnes, "A review of wave-energy extraction," *Marine Structures*, vol. 20, pp. 185–201, 2007.
[58] J. Isberg, J. Engström, and M. Leijon, "Depth variation of energy transport in fluid gravity waves," *Journal of Renewable and Sustainable Energy*, vol. 2, 2010.
[59] M. Penalba, G. Giorgi, and J. Ringwood, "Mathematical modelling of wave energy converters: A review of nonlinear approaches," *Renewable and Sustainable Energy Reviews*, vol. 78, pp. 1188–1207, 2017.
[60] "https://www.comsol.com/cfd-module," 2017-06-29.
[61] "http://www.ansys.com/products/fluids/ansys-fluent," 2017-06-29.
[62] "https://cfd.direct/openfoam/user-guide/introduction/," 2017-06-29.
[63] H. Wolgamot and C. Fitzgerald, "Nonlinear hydrodynamic and real fluid effects on wave energy converters," *In Proc IMechE, Part A: J Power and Energy (2015)*, 2015.
[64] N. Jacobsen, D. Fuhrman, and J. Fredsoe, "A wave generation toolbox for the open-source cfd library: Openfoam," *International Journal for Numerical Methods in Fluids*, vol. 70, pp. 1073–1088, 2012.
[65] T. Adcock, P. Taylor, S. Yan, Q. Ma, and P. Janssen, "Did the draupner wave occur in a crossing sea?," *Proceedings of the Royal Society - A*, vol. 467, pp. 3004–3021, 2011.
[66] Y. Li and Y. Yu, "A synthesis of numerical methods for modeling wave energy converter-point absorbers," *Renewable and Sustainable Energy Reviews*, vol. 16, pp. 4352–4364, 2012.
[67] K. Budal and J. Falnes, "Power generation from ocean waves using a resonant oscillating system," *Marine Science Communication*, vol. 1, pp. 269–288, 1975.
[68] J. Newman, "The exciting forces on fixed bodies in waves," *Journal of Ship Reasearch*, vol. 6(3), pp. 10–17, 1962.
[69] R. Yeung, "Added mass and damping of a vertical cylinder in finite-depth waters," *Applied Ocean Research*, vol. 3, pp. 119–133, 1980.
[70] A. Hulme, "The wave forces acting on a floating hemisphere undergoing forced periodic oscillations," *Journal of Fluid Mechanics*, vol. 121, pp. 443–463, 1982.
[71] P. McIver, "Wave forces on arrays of floating bodies," *Journal of Engineering Mathematics*, vol. 18(4), pp. 273–285, 1984.

[72] P. Siddorn and E. Taylor, "Diffraction and independent radiation by an array of floating cylinders," *Ocean Engineering*, vol. 13, pp. 1289–1303, 2008.
[73] M. Göteman, J. Engström, M. Eriksson, and J. Isberg, "Optimizing wave energy parks with over 1000 interacting point-absorbers using an approximate analytical method," *International Journal of Marine Energy*, vol. 10, pp. 113–126, 2015.
[74] C. Lee, *WAMIT theory manual*. Cambridge, MA: Departure of Ocean Engineering, Massachusetts Institute of Technology, http://www.wamit.com/manual.htm, accessed 2017-06-29, 1995.
[75] M. Longuet-Higgins and E. Cokelet, "The deformation of steep surface waves on water. i. a numerical method of computation," *Proceedings of the Royal Society of London*, vol. A350, pp. 1–26, 1976.
[76] M. Longuet-Higgins and E. Cokelet, "The deformation of steep surface waves on water .ii. growth of normal-mode instabilities," *Proceedings of the Royal Society of London, A Mathematical and Physical Science*, vol. 364(1716), 1978.
[77] C. Mei, "Wave extraction from water waves," *Journal of Ship Reasearch*, vol. 20, pp. 63–66, 1976.
[78] D. Evans, "A theory for wave power absorption by oscillating bodies," *Journal of Fluid Mechanics*, vol. 77, pp. 1–25, 1976.
[79] J. Newman, "The interaction of stationary vessels with regular waves.," *In: Proceedings of the 11th symposium on naval hydrodynamics*, pp. 491–501, 1976.
[80] K. Budal and J. Falnes, "Interacting point absorbers with controlled motion," *Power from Sea Waves*, pp. 381–399, 1980.
[81] M. McIver and P. McIver, "Water waves in the time domain," *Journal of Engineering Mathematics*, vol. 70, pp. 111–128, 2011.
[82] M. Eriksson, J. Isberg, and M. Leijon, "Hydrodynamic modelling of a direct drive wave energy converter," *International Journal of Engineering Science*, vol. 43, pp. 1377–1387, 2005.
[83] W. Cummins, "The impulse response function and ship motions," *Schiffstechnik*, vol. 9 1661, pp. 101–109, 1962.
[84] E. Jefferys, "Device characterisation," *Power from Sea Waves*, pp. 413–438, 1980.
[85] C. Eskilsson, A. Bosi, and M. Ricchiuto, "Wave induced motion of point-absorbers: a hierarchial investigation of hydrodynamic models," *In proceedings of the 11th European Wave and Tidal Energy Conference Series EWTEC, Nantes, France*, 2015.
[86] J. Davidson, S. Giorgi, and J. Ringwood, "Linear parametric models for wave enrgy converters identified from numerical wave tank experiments," *Ocean Engineering*, vol. 103, pp. 31–39, 2015.
[87] J. Davidson, S. Giorgi, and J. Ringwood, "Identification of wave energy device models from numerical wave tank data - part 1: Numerical wave tank identification tests," *IEEE Transactions on Sustainable Energy*, vol. 7, pp. 1012 – 1019, 2016.
[88] P. Schmitt and B. Elsaesser, "On the use of openfoam to model oscillating wave surge converters," *Ocean Engineering*, vol. 108, pp. 98–104, 2015.

[89] Y. Yu and Y. Li, "Reynolds-averaged Navier-Stokes simulation of the heave performance of a two-body floating-point absorber wave energy system," *Computers & Fluids*, vol. 73, pp. 104–114, 2013.
[90] E. Ransley, *Survivability of Wave Energy Converter and Mooring Coupled System using CFD*. PhD thesis, Plymouth University, 2015.
[91] E. Ransley, D. Greaves, A. Raby, D. Simmonds, and M. Hann, "Survivability of wave energy converters using CFD," *Renewable Energy*, vol. 109, pp. 235–247, 2017.
[92] E. Ransley, D. Greaves, A. Raby, D. Simmonds, M. Jakobsen, and M. Kramer, "RANS-VOF modelling of the wavestar point absorber," *Renewable Energy (2017)*, vol. 109, pp. 49–65, 2017.
[93] W. Chen, I. Dolguntseva, A. Savin, Y. Zhang, W. Li, O. Svensson, and M. Leijon, "Numerical modelling of a point-absorbing wave energy converter in irregular and extreme waves," *Applied Ocean Research*, vol. 63, pp. 90–105, 2017.
[94] W. Craig, "Surface water waves and tsunamis," *Journal of Dynamics and Differential Equations*, vol. 18, 2006.
[95] R. LeVeque, D. George, and M. Berger, "Tsunami modelling with adaptively refined finite volume methods," *Acta Numerica*, pp. 211–289, 2011.
[96] N. Shuto, "Numerical simulation of tsunamis - its present and near future," *Natural Hazards*, vol. 4, pp. 171–191, 1991.
[97] N. Shuto, "The Nihonkai-chubu eartquake tsunami on the north Akita coast," *Coastal Engineering in Japan*, vol. 28, pp. 255–264, 1985.
[98] W. Allsop, I. Chandler, and M. Zaccaria, "Improvements in the physical modelling of tsunamis and their effects," in *Proc 5th Int. Conf. on the Application of Phys. Modelling to Port and Coastal Protection, Bulgaria*, 2014.
[99] M. Shito, I. Inuzuka, I. Amaya, H. Saito, and J. Kurata, "Numerical simulations and experiments on tsunami for the design of coastal and offshore structures," *IHI Engineering Review*, vol. 46, pp. 21–25, 2014.
[100] J. Bricker and A. Nakayama, "Contribution od trapped air, deck superelevation, and nearby structures to bridge deck failure during a tsunami," *Journal of hydraulic engineering*, 2014.
[101] Hartana, Murakami, Yamaguchi, and Maki, "2-phase flow analysis of tsunami forces acting on bridge structures," *Journal of Japan Society of Civil Engineers, Ser. B3 (Ocean Engineering)*, vol. 69, 2013.
[102] S. Douglas and I. Nistor, "On the effect of bed condition on the development of tsunami-induced loading on structures using openfoam," *Natural Hazards*, 2015.
[103] B. Seiffert and R. Ertekin, "Numerical modeling of solitary and cnoidal waves propagating over a submerged bridge deck," *OCEANS, 2012 - Yeosu, South Korea*, 2012.
[104] L. OBrien, P. Christodoulides, E. Renzi, T. Stefanakis, and F. Dias, "Will oscillating wave surge converters survive tsunamis?," *Theoretical and Applied Mechanical Letters*, vol. 5, pp. 160–166, 2015.
[105] P. Madsen, D. Furman, and H. Shäffer, "On the solitary wave paradigm for tsunamis," *Journal of Geophysical research*, vol. 113, 2008.

[106] O. Danielsson, M. Leijon, and E. Sjöstedt, "Detailed study of the magnetic circuit in a longitudinal flux permanent-magnet synchronous linear generator," *IEEE Transactions on Magnetics*, vol. 41, pp. 2490–2494, 2005.

[107] M. Hann, D. Greaves, and A. Raby, "Snatch loading of a single taut moored floating wave energy converter," *Ocean Engineering*, vol. 96, pp. 258–271, 2015.

[108] H. Gravråkmo, M. Leijon, E. Strömstedt, J. Engström, S. Tyrberg, A. Savin, O. Svensson, and R. Waters, "Description of a torus shaped buoy for wave energy point absorber," *Proceedings of Renewable Energy, Pacifico Yokohama, Yokohama, Japan*, 2010.

[109] L. Hai, V. Castellucci, E. Lejerskog, R. Waters, and M. Leijon, "Force in the connection line for a wave energy converter: Simulation and measurement experimental setup," *Proceedings of ASME 2014 33rd International Conference on Ocean, Offshore and Arctic Engineering, San Fransisco, USA*, 2014.

Acta Universitatis Upsaliensis

Digital Comprehensive Summaries of Uppsala Dissertations from the Faculty of Science and Technology 1551

Editor: The Dean of the Faculty of Science and Technology

A doctoral dissertation from the Faculty of Science and Technology, Uppsala University, is usually a summary of a number of papers. A few copies of the complete dissertation are kept at major Swedish research libraries, while the summary alone is distributed internationally through the series Digital Comprehensive Summaries of Uppsala Dissertations from the Faculty of Science and Technology. (Prior to January, 2005, the series was published under the title "Comprehensive Summaries of Uppsala Dissertations from the Faculty of Science and Technology".)

Distribution: publications.uu.se
urn:nbn:se:uu:diva-328499

ACTA
UNIVERSITATIS
UPSALIENSIS
UPPSALA
2017